Geothermics xxx (xxxx) xxx

Contents lists available at ScienceDirect

Geothermics

journal homepage: www.elsevier.com/locate/geothermics

Fluid geochemistry of the Los Humeros geothermal field (LHGF - Puebla, Mexico): New constraints for the conceptual model

Matteo Lelli [a,*], Thomas Gunter Kretzschmar [b], Jacopo Cabassi [c], Marco Doveri [a], Juan Ignacio Sanchez-Avila [b,d], Fabrizio Gherardi [a], Gabriella Magro [a], Francesco Norelli [a]

[a] Institute of Geosciences and Earth Resources, National Research Council, Via G. Moruzzi 1, 56124, Pisa, Italy
[b] Center for Scientific Research and Higher Education, Carr Tijuana-Ensenada 3918, 22860, Ensenada, B.C., Mexico
[c] Institute of Geosciences and Earth Resources, National Research Council, Via G. La Pira, 50121, Firenze, Italy
[d] Research Centre for Toxic Compounds in the Environment (RECETOX), Faculty of Science, Masaryk University, Kamenice 753/5, 625 00, Brno, Czech Republic

ARTICLE INFO

Keywords:
Fluid geochemistry
Chemical and isotopic characterization
Groundwater flow paths
Geothermal exploration
Conceptual model
Los Humeros geothermal field

ABSTRACT

Geothermal power in Mexico is mainly produced in four geothermal fields operated by the Comision Federal de Electricidad (CFE): Cerro Prieto, Los Azufres, Los Humeros, and Las Tres Virgenes. The Los Humeros Geothermal Field (LHGF) is ranked third in terms of generated capacity, and in the last decade its installed capacity has doubled (up to 95.0 MW). Further increases in the geothermal power generation capacity in Mexico are planned, and thus the LHGF warrants further examination. The development and growth phases of any geothermal project must start from an awareness of the conceptual model of the natural system studied. The recharge mechanism, feeding zones, and fluid flow-path must be identified, along with the estimation of the temperature at the productive level and of phase separation (liquid – steam). To accomplish this, detailed fluid geochemical surveys were carried out in June 2017 and March 2018, in which 57 and 87 samples were collected, respectively, from cold and thermal springs, water wells and maar lakes located around and inside the LHGF. Samples from fumaroles inside the producing area were also collected for the first time, together with fluid from re-injection wells. The presence of a meteoric component, which plays an important role at the regional scale, is confirmed by the chemical and isotope data, and its contribution in terms of recharge may be higher than previously assumed. The Sierra Madre Oriental, on the west side of the LHGF, is characterized by widespread outcrops of limestone belonging to the same geological formation as those at the bottom of the LHGF. The isotope composition (δD and $\delta^{18}O$, respectively -77.3‰ and -10.50‰ for the hypothetical Infiltration Water - IW) is similar to that observed in cold springs located in the Sierra Madre Oriental, and from this the evolution of isotopes in the liquid-rock-steam system during water-rock interaction and phase separation processes can be modelled. Thus, the experimental data obtained for natural gas emissions (fumarolic condensates) and for geothermal fluids can be reproduced. These findings suggest that geothermal fluids in the LHGF are likely to be derived from meteoric water infiltrating (IW) the limestone outcrops of the Sierra Madre Oriental. During their flow-path, the infiltrating waters exchange isotopes at a high temperature with the crustal rocks, which have a much higher $^{18}O/^{16}O$ ratio, resulting in a shift towards higher $\delta^{18}O$ (-4.35‰ ± 1) as the water O exchanges with rock O. The vapor phase can be separated from this deep water (DW) and it is discharged from the fumarolic effluents of Loma Blanca. Single Step Vapor Separation (SSVS) and Continuous Steam Separation processes (CSS) were modelled using stable isotopes of water. The results of geochemical modeling agree with available data for geothermal liquids discharged from several geothermal wells, suggesting that steam separation may be interpreted either as SSVS or CSS. Other processes can affect the chemistry and isotope composition of geothermal fluids (e.g. phase segregation, gas exchange, contributions from magmatic-volcanic deep fluids and re-injection fluids). The proposed conceptual model is consistent with both the geochemical data and the geological setting, and provides a useful point of reference for examining the fluid flow-path and geochemical processes active in the LHGF, at least at a general level.

* Corresponding author.
E-mail address: m.lelli@igg.cnr.it (M. Lelli).

https://doi.org/10.1016/j.geothermics.2020.101983
Received 3 February 2020; Received in revised form 9 October 2020; Accepted 12 October 2020

An involvement of magmatic-volcanic deep fluids in the feeding mechanism of the geothermal system cannot be excluded at priori, but the regional meteoric end-member is supported by the data and it seems the most important component.

1. Introduction

The Los Humeros Geothermal Field (LHGF) is located 200 km SE of Mexico City and is one of the most important Mexican geothermal systems for electric power generation (ca. 95.0 MW – Gutiérrez-Negrín, 2019). Maximum temperatures close to 400 °C were measured in geothermal wells located in the northern part of the producing area. A condition of excess enthalpy (>2400 KJ/Kg - Gutierrez-Negrin and Izquierdo-Montalvo, 2010) has characterized the LHGF since the first stage of fluid extraction (started in 1982 - Arellano et al., 2015) and was enhanced by power production (started in 1990; Arellano et al., 2003), causing aquifer boiling, phase separation and steam condensation (Barragán et al., 2008; Arellano et al., 2015). From 1982 to December 2012, about 123 Mt of fluid were extracted (Arellano et al., 2015), with around 104 Mt of steam (84.3 %) and 19 Mt of liquid (15.7 %). Re-injection started in 1995 and up to December 2012 about 6.3 Mt of extracted fluid was re-injected in the reservoir (Arellano et al., 2015). This represents a small fraction of the total extracted fluid (5.1 %), and thus the effectiveness of re-injection in LHGF has not been clearly identified, even if the production of steam or condensed steam from boiling of reinjected fluids was identified in a number of wells (Arellano et al., 2015; Pinti et al., 2017). Similarly, the recharge mechanism has been a subject of debate, and i) Prol-Ledesma (1998) first proposed possible recharge from the permeable limestone of the Sierra Madre Oriental and the Citlaltepetl volcano; ii) Cedillo-Rodrigez (2000) considered the LHGF to be isolated from the regional recharge and fed only by rainfall infiltration inside the Los Humeros Caldera Collapse; and iii) more recently, others (Tello et al., 2000; Barragán et al., 2010; Pinti et al., 2017) have considered the geothermal fluids in Los Humeros as the result of mixed end-members, in which andesitic water (as defined by Giggenbach, 1992a) represents a very important component (up to ~50 %). In these works (Tello et al., 2000; Barragán et al., 2010; Pinti et al., 2017), although the andesitic water is considered one of the main end-members, significant discrepancies characterize the isotope composition of the inferred meteoric component.

Extensive geochemical data regarding the characterization of geothermal fluids from producing wells has been obtained, and important chemical and isotopic temporal evolution, due to geothermal production in the LHGF, has been identified (Barragán et al., 1988, 1989, 1991; Truesdell, 1991a, b; Prol-Ledesma, 1998; Arellano et al., 1998, 2003, 2015). However, very little or no geochemical data about cold water from springs and wells are available for the identification of the feeding zones and the mean altitudes of the recharge areas. Establishing these factors is essential for the effective management and monitoring of active power plants, and for future planning.

To address these uncertainties and lack of information, a detailed hydro-geochemical study was conducted in the LHGF, in which physico-chemical and isotopic parameters were determined in cold and thermal waters from springs, wells, and maar lakes located around and inside the LHGF producing area. Fumaroles may represent geothermal fluids less influenced by power production activities (as they are natural manifestations), and samples from the most suitable fumaroles present inside the Los Humeros producing area were thus collected for the first time. This can provide key information concerning the stable isotope composition of the condensed steam, so it can be linked to secondary cooling processes (boiling and vapor loss) that take place during the rise of deep geothermal fluids.

2. The geological and hydrogeological settings of the LHGF

The LHGF is located in the eastern portion of the Trans-Mexican Volcanic Belt (TMVB, Miocene-Holocene, Ferrari et al., 2012), near the border of the Sierra Madre Oriental province (Fig. 1).

The LHGF producing area is within a complex caldera system (Ferriz and Mahood, 1984), with a mean altitude of about 2800−2900 m.a.s.l. The basement of the LHGF is composed of Paleozoic granites and schists (Romero, 1991), covered by Mesozoic metamorphosed limestones (De la Cruz, 1983; Carrasco-Núñez et al., 2017a). At around 10 Ma, the Los Humeros area was characterized by volcanic activity, and fractured andesites and basaltic lavas were emitted, forming the thick (up to 800−900 m) Cuyuaco and Alseseca units (Cedillo-Rodríguez, 1984; López-Hernández, 1995; Yáñez and Garcia, 1982). Other volcanic activity took place between 5 and 1.55 Ma, forming the Teziutlán unit that is composed of fractured andesites with a thickness >1500 m (Yáñez and Garcia, 1982; Ferriz and Mahood, 1984; Carrasco-Núñez et al., 2017a, 2017b). The caldera complex system is composed of two main calderas and is related to the volcanic activity that began 460 ky ago and continued until 20 ky ago. The Los Humeros caldera (21 × 15 km) formation belongs to the older period and is associated with a large eruption (involving about 115 km^3) that emplaced the rhyolitic Xaltipan ignimbrite (Ferriz and Mahood, 1984). The second caldera formation event produced the Los Potreros caldera, associated with the emplacement of the rhyodacitic-andesitic Zaragoza ignimbrite (Carrasco-Núñez and Branney, 2005; Carrasco-Núñez et al., 2012), which is about 60–140 ky old (Dávila-Harris and Carrasco-Núñez, 2014; Carrasco-Núñez et al., 2018). Caldera formation events were followed by various intracalderic explosive and effusive phases, associated with the emplacement of rhyolitic and dacitic domes, basaltic-andesitic and trachyandesitic lava flows, and dacitic, trachydacitic, andesitic, and basaltic pumice and scoria fall deposits (Ferriz and Mahood, 1984; Dávila-Harris and Carrasco-Núñez, 2014; Norini et al., 2015; Carrasco-Núñez et al., 2017a, 2017b).

Currently, the LHGF has an installed electric power capacity of about 95 MW (Gutiérrez-Negrín, 2019) and commercial production began in 1990, although fluid extraction started in 1982 (Arellano et al., 2015). Productive levels are mainly located in the andesite and basalts of the Cuyuaco, Alseseca and Teziutlán units, which overlap with low-permeable Quaternary ignimbrite (e.g. 600 m thick Xaltipan ignimbrite associated with the caldera formation: Cedillo-Rodríguez, 1997, 1999; Arellano et al., 2003; Lorenzo-Pulido, 2008; Gutiérrez-Negrín and Izquierdo-Montalvo, 2010). LHGF is generally characterized by low permeability conditions, although the presence of two main system faults (aligned NW-SE to N–S and NE-SW to E–W, respectively) contribute to enhancing the permeability (Cedillo-Rodríguez, 2000; Pinti et al., 2017). Surface natural manifestations consist of weak gas emissions (steaming ground and vents) localised 1) in the crater of Xalapazco, 2) close to Los Humeros village, and 3) in Loma Blanca, in the southern, central, and northern parts of the LH producing area, respectively (Casique et al., 1982).

3. Sampling and laboratory analysis

To obtain insights into the mechanisms of recharge, fluid flow-paths and physical-chemical processes affecting the LH geothermal system, a geochemical survey including both chemical and isotope analysis was conducted on samples from water points (springs, water wells, lakes) and natural gas manifestations in the LHGF area and its surroundings. For geothermal wells we referred to the extensive geochemical data

available from the CFE, which monitors the state and evolution of the geothermal field, and also to other studies (Tello, 1990; Arellano et al., 2003; Tello et al., 2005).

3.1. Waters

Two sampling surveys were conducted in the LHGF in June 2017 and March 2018, through which 57 and 87 water samples were collected, respectively, from cold springs, cold water wells, maar lakes, thermal springs, and reinjection wells. For a better understanding of the recharge mechanisms of the LHGF, specific cold springs on the surrounding hills were selected and sampled (e.g. Cofre de Perote, Sierra Madre Oriental) at different altitudes. As similar studies show (Doveri and Mussi, 2014; Mnjokava et al., 2018), this procedure is useful for defining the water isotope signature of the infiltration water in different sectors and altitude ranges within the area studied, and thus supports the interpretation of the isotope signature of the geothermal fluids. Other cold springs and wells sampled in the area overlap with sampling points of previous monitoring networks, whereas in other cases we considered new and hitherto un-investigated points. The sampling points are shown on the location map in Fig. 2. The samples collected cover a wider area than in previous investigations (Portugal et al., 1994; Barragán et al., 1998; Tello et al., 2000), and include different kinds of lithologies, thus increasing the hydrogeochemical knowledge of the region.

The temperature, pH, electrical conductivity, redox potential, and dissolved oxygen were measured directly in the field, using suitable portable instruments. The total alkalinity was also determined *in situ* by an acid-base titration, using a micro-dosimeter containing HCl 0.1 N with methyl-orange as the pH-indicator. When possible, the flow rate of the springs was measured using a flow-meter or other suitable vessel. All parameters measured in the field are reported in Table 1 (Supplementary material), together with the GPS coordinates and altitude data. Several aliquots were collected, using a specific treatment to preserve the chemical parameters before the laboratory analysis, including a filtered sample (0.45 µm membranes of cellulose acetate) for determining Cl, NO_3, SO_4, F, and Br; a filtered and acidified sample (0.45 µm membranes of cellulose acetate and HNO_3 1:1 suprapure) for determining Na, K, Ca, Mg, B, Li, Sr, and SiO_2; and a non-treated sample for water-isotope analysis (δD, $\delta^{18}O$, tritium). The chemical and isotope analysis was conducted in the IGG-CNR labs in Pisa (Italy), using Inductively Coupled Plasma-Optical Emission Spectroscopy (Na, K, Ca, Mg, B, Li, Sr), Ion Chromatography (Cl, SO_4, NO_3, Br), Potentiometry equipped with ion-selective electrodes (F), Spectrophotometry UV-Vis (SiO_2), Liquid Water Isotope Analysis based on the Off-Axis Integrated Cavity Output Spectroscopy (δD and $\delta^{18}O$), and Liquid scintillator counting (tritium). The short-term analytical precision (repeatability) was better than 2% for the ICP-OES analyses, 3–5 % for IC and ISE determinations, and close to 5% for visible spectrophotometry. The uncertainties for the $\delta^{18}O$ and δD values were ±0.05‰ and ±1‰, respectively.

The results of the water analysis are shown in Table 2 (Supplementary material). Chemical data are shown in mg/L, whereas the O and H stable isotope results are reported using delta values in ‰ versus Vienna Standard Mean Ocean Water (VSMOW). The charge balance is also reported, and was lower than 3% for all samples.

3.2. Gases

The LHGF, including the central hottest part of the producing area, is characterized by a lack of intense fumarolic manifestations. Diffuse degassing from soils represents most of the diffused natural gas manifestations (Peiffer et al., 2018). However, steaming ground and weak steam vents are also present in some areas: Cueva Ahumada (50 °C) in the Xalapazco crater, Los Humeros (70 °C), and Loma Blanca (80 °C) (Casique et al., 1982). Geothermal fluids from natural steam/gas vents may be less affected by power production, and so key parameters can be calculated (e.g. the temperature of the liquid phase from which the gas phase is released, the temperature at which the phase separation process occurs, and the gas/steam ratio). These are required to define the thermodynamic equilibrium conditions present at depth (in the gas equilibration zone, which can represent reservoir conditions, or shallower ones if re-equilibration of the gas phase takes place during its rise towards the surface) and to identify any secondary cooling processes (boiling and steam condensation) that take place during the rise of deep geothermal fluids. No chemical and isotope data is available for the natural steam/gas vents in the LHGF, so in this study particular attention was given to the sampling and analysis of these natural thermal manifestations.

In March 2018, two sites with suitable fumaroles were identified for the collection of gas samples: two aliquots in Loma Blanca (LB1) and one

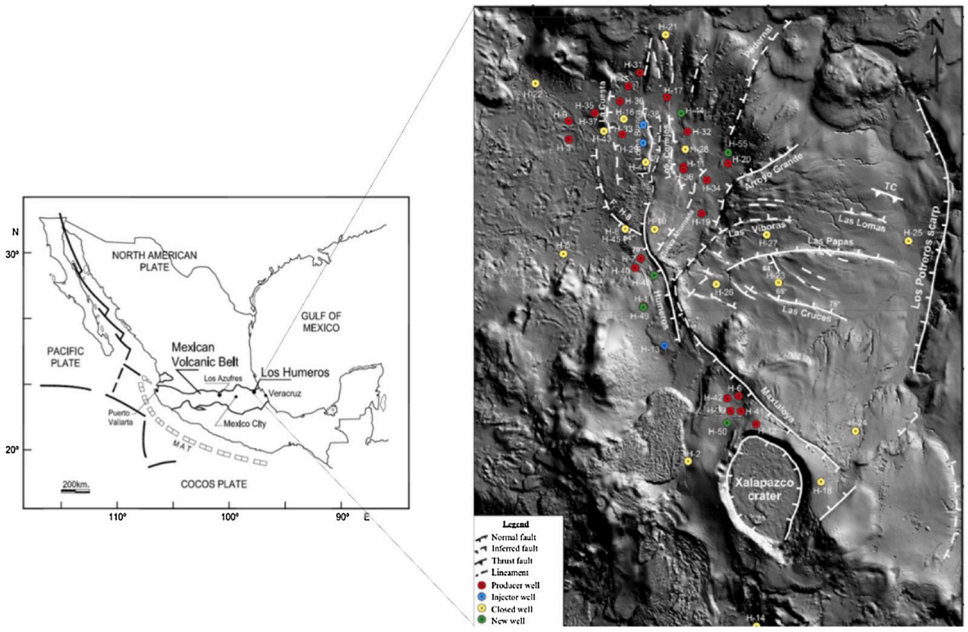

Fig. 1. Location of the LHGF. Sketch of the Los Humeros Digital Elevation Model is from Carrasco-Núñez et al., 2017a (modified).

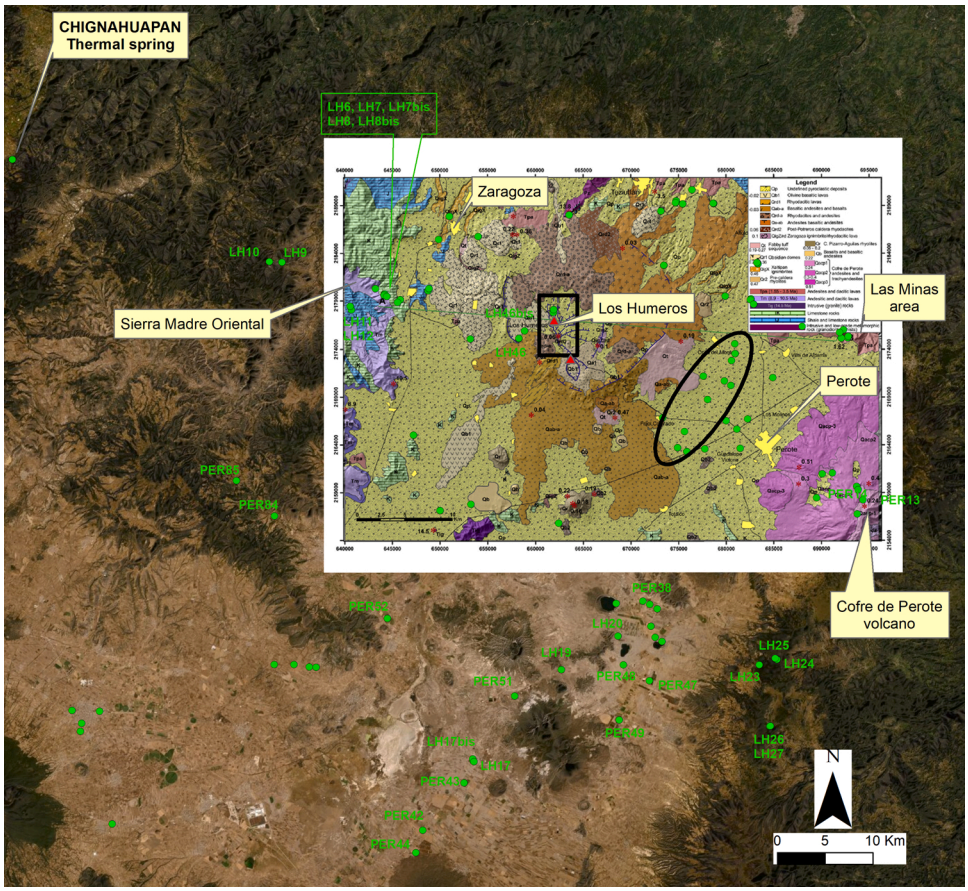

Fig. 2. Location map of collected water (dots) and gas samples (collected natural gas emissions are located close to the Los Humeros village, see the triangles). The polygon close to the Los Humeros village represents the perimeter of the main producing area of LHGF, whereas the ellipse delimits the water wells located in the Perote plain and characterized by T>20 °C. Revised geologic map of Los Humeros is also reported (modified from Ferriz and Mahood, 1984; De la Cruz, 1983; Yáñez and García, 1982). The satellite image is from Esri ArcGIS World Imagery.

in Xalapazco (XA1) (triangles in Fig. 2). The first gas manifestation is located in Loma Blanca, 200−300 m north of the Los Humeros village, while the second is inside the Xalapazco crater on the southern part of the producing area. Loma Blanca is a small altered area in which weak fumarolic emissions are present, with a maximum temperature of 92.8 °C (boiling temperature at the local altitude ≈ 2800 m.a.s.l.). In Xalapazco, gas emissions and steaming ground with a maximum temperature of 64.5 °C characterize a small area on the inner northern side of the crater.

In Loma Blanca, gas sampling was performed using Giggenbach bottles partially filled with a sodium hydroxide solution (≈4.5 N) and then evacuated to remove the atmospheric air (Giggenbach, 1975). With this sampling method, steam and gas reactive species (as CO_2 and H_2S) are dissolved in a NaOH aqueous solution, while other incondensable gases (such as Ar, H_2, O_2, N_2, CH_4, He) can accumulate in the headspace of the Giggenbach bottles. However, this method is not suitable for analyzing the carbon monoxide concentration, so other aliquots were collected. A suitable quartz sampling line was used for steam condensation, thus separating the condensable from the incondensable proportions (Cioni et al., 1988). The incondensable gases were stored in suitable dry glass bottles equipped with two stopcocks, while the condensed steam was stored in plastic bottles with double caps. Samples for He and Ne isotope determination were collected using Cu-tubes and suitable metal clamps.

All gas analyses were performed in the IGG-CNR laboratories in Pisa. Non-condensable inorganic gases were determined in the headspace of glass bottles containing aqueous solutions of NaOH and in dry gas bottles, using a gas-chromatograph equipped with a 30 m-long 5 Å molecular sieve capillary column (I.D. 0.53 mm) and a Thermal Conductivity Detector (TCD). Low CH_4 concentrations (<10 ppmv) were measured using the same gas-chromatograph plus a Flame Ionization Detector (FID). The alkaline solution was analyzed for H_2S and CO_2 concentrations, using an ion-chromatograph and an automatic titrator, respectively (after oxidation with hydrogen peroxide). Carbon dioxide and H_2S in the dry gas bottles were determined using a gas-chromatograph equipped with a packed Chromosorb column and a Thermal Conductivity Detector (TCD). The carbon monoxide concentration in the dry gas bottles was determined by means of a gas-chromatograph equipped with a packed molecular sieve (5 Å, 80/100 mesh) column (3 m long, using He as the carrier gas) and a high-sensitivity reduced gas detector (HgO; detection limit 0.05 ppmv). Analysis of $\delta^{13}C$ CO_2 (‰ VPDB – Vienna Pee Dee Belemnite) was conducted on the dry gas bottle samples via a GC-combustion interface coupled with a mass spectrometer for establishing the isotope ratio (Trace GC Ultra – Thermo Scientific). Noble gases (He and Ne) were analyzed for determine their levels and isotope composition, following the procedure of Magro et al. (2003). The extraction line was connected to both a magnetic mass spectrometer and a quadrupole mass spectrometer. All the chemical data obtained had analytical uncertainties of ≤ 5% for the main gas components and ≤ 10 % for minor and trace gas species. The uncertainties for carbon isotopes were ±0.1‰, while the isotope analyses of noble gases give a reproducibility of better than 10 % over the analysis period. Chemical and isotope data are shown in Table 3 (Supplementary material).

4. Results and discussion

4.1. Waters

4.1.1. Hydrogeochemical classification and binary plots

The water chemistry was analyzed in terms of relative concentrations of major anions (HCO_3, SO_4, and Cl) and cations (Na, K, Ca, and Mg), by means of triangular diagrams (Giggenbach, 1988). The triangular

classification plots (Fig. 3a and b) show that most of the collected water had HCO_3 and Na or Ca as the dominant anion and cation dissolved species, respectively. The chemical composition for the geothermal fluids of Los Humeros is known to depend on the depth of the well waters and on well-head enthalpy (Arellano et al., 2003). The chemical data of geothermal wells were also included for reference in the ternary diagrams, after selecting those characterized by a relatively small ionic unbalance (<7.5 %). The chemistry of geothermal fluids is mainly represented by a Na-bicarbonate composition, and to a lesser extent by Na−Cl and Na−SO_4(Cl) fluids.

The ternary diagrams enable the identification of three main "hydrochemical types": 1) Na−HCO_3, 2) Ca−HCO_3 and 3) Ca−SO_4(HCO_3) waters. The first is represented by spring waters located at a high altitude in the Cofre de Perote volcano (e.g. PER13 and PER14) or close to the Zaragoza village, in which outcrops of lava rocks (i.e., andesites, trachyandesites, dacites) are extensively present (see geological map in Fig. 2). This represents the first stage of water-rock interaction between meteoric water and andesites. The second hydrochemical type (i.e. Ca−HCO_3) represents waters coming from cold springs and wells located at different altitudes. This illustrates the various evolution stages in the interaction between meteoric waters and carbonates. Samples such as LH6, LH7, LH7bis, LH8 and LH8bis, were located on or close to limestone outcrops, in particular on the western side of the study area (Sierra Madre Oriental). The third hydrochemical type (Ca−SO_4−HCO_3) characterizes some well waters (LH17, LH17bis and PER43) located in the south part of the studied area close to the "Totolcingo lagoon", in which higher SO_4 concentrations are present. Very dry to arid climate conditions characterize this region and cause intense evapotranspiration/evaporation. A widespread mineral salt deposition is present around the lagoon, known as *"Tequesquite"*, which is mainly composed of sodium-carbonate and sodium-chloride with associated potassium-carbonate, sodium-sulfate and clay (Alcocer and Hammer, 1998). The Ca−SO_4−HCO_3 hydrochemical type may reflect the interaction at surface levels of meteoric water with a Tequesquite salt incrustation. This process appears to involve samples from wells located close to maar lakes (i.e. LH20, PER38 and PER48), in which the Total Ionic Salinity (T.I.S.) is higher than in other samples (Fig. 4a and b). Excluding the very saline water coming from the Alchichica maar lake (T.I.S. = 320 meq/L), which is the result of intense evaporation, the T.I.S. values for the other samples range from 0.7 to 3.4 meq/L for cold springs, from 0.5–114 meq/L for well waters and from 5.2–9.8 meq/L for surface water from creeks/streams.

On the Perote plain (mean altitude ~2400 m.a.s.l.) a cluster of wells characterized by warm waters (Na−Ca−HCO_3) with temperatures ranging from 20 °C to 33.1 °C (LH50, LH50bis, LH54, LH55, LH61, PER27, PER31, PER54, PER55, PER56, PER57 and PER59 – included in the ellipse in Fig. 2) were identified. These wells are utilized by farms and have depths ranging from 120 to 180 m and a flow rate of about 60−80 L/sec. Productive levels are located in rock formations, probably represented by andesite and dacite lavas at a shallow level close to Perote (see the geological map and the structural stratigraphic section reported in Carrasco-Núñez et al., 2017a). The T.I.S. values for these "warm well waters" range from 16 meq/L to 44 meq/L. Although the results for these samples can be interpreted as the result of interactions between meteoric water and andesite rocks, their physical-chemical characteristics (in particular the temperature and salinity) differ from those of the other Na−HCO_3 waters. Figs. 4a and b support this finding, as warm well waters from the Perote plain show a separate trend from waters characterized by higher T.I.S. values (i.e. PER51, PER78, LH17, LH17bis, PER43, PER38 and PER48). However, the most saline waters from warm wells (e.g. LH54 and LH55) show a similar pattern in some of the binary plots (e.g. Na vs Cl, K vs Cl, Li vs Cl and B vs Cl – Fig. 5a-d). The interpretation of the data is not unequivocal and more data is required to forward a specific hypothesis.

4.1.2. *Hydrogen and oxygen stable isotopes*

Extensive data on the isotope composition of the oxygen and hydrogen in cold spring and geothermal well waters have been collected from the LHGF during previous research campaigns (Portugal et al., 1994; Barragán et al., 1998; Tello et al., 2000). However, no detailed study on isotope hydrology has as yet been conducted. In this study, samples were collected specifically from springs located at different altitudes around the LH caldera, including those near the top of the Cofre de Perote volcano (≈4000 m.a.s.l.) and in the Sierra Madre Oriental (see Fig. 1). The δD and $\delta^{18}O$ values for the water samples collected in the LHGF and its surroundings are given in the correlation diagram in Fig. 6, together with the Global Meteoric Water Line (GMWL – $\delta D = 8 \cdot \delta^{18}O + 10$, Craig, 1961) and the Meteoric Water Line (MWL) for central Mexico (parallel to the GMWL, but having d = 5−7‰ - Issar et al., 1984).

In general, waters from springs plot along the GMWL whereas those from cold wells plot towards the MWL. Partial evaporation in semi-arid conditions (typical of the southern part of the area studied) and/or the recycling of water during irrigation (which obviously only affects the

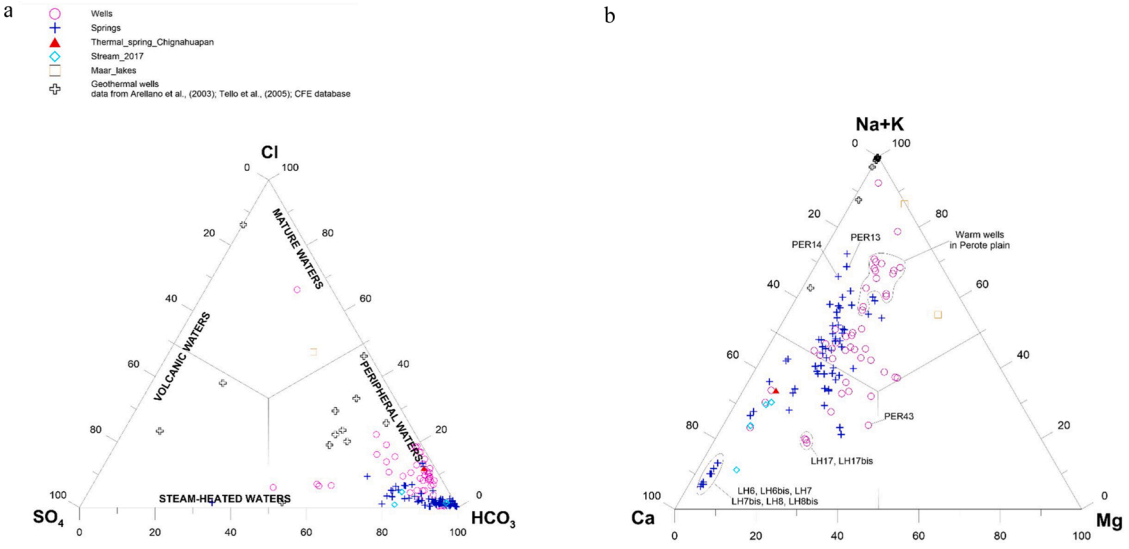

Fig. 3. (a) Classification triangular plot HCO_3-Cl-SO_4 for water samples collected. (b) Classification triangular plot (Na + K)-Ca-Mg for water samples collected. Symbols as in Fig. 3a.

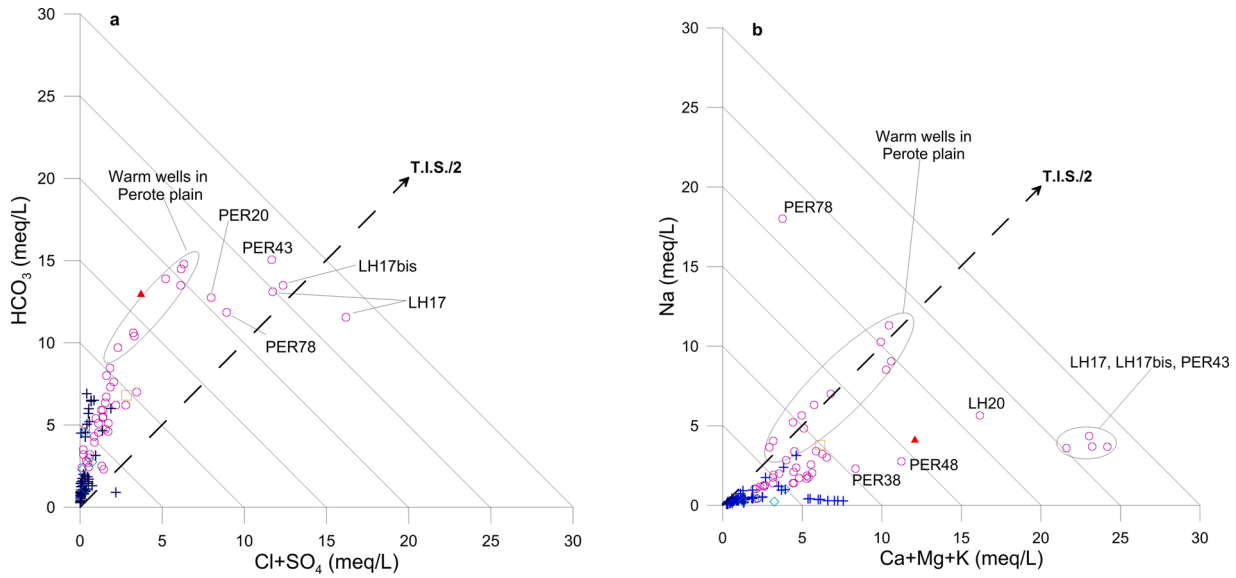

Fig. 4. Correlation plots (a) HCO_3 vs. $(Cl + SO_4)$ and (b) Na vs. $(Ca + Mg + K)$ for water samples collected. The iso-salinity lines are also reported. Symbols as in Figure 3a.

waters from wells) may lead to this. In addition, the samples show a wide variation in the isotope composition due to different infiltration altitudes. Although δD and $\delta^{18}O$ have a large range of values, several samples collected outside the LH caldera (e.g. LH12, LH13, LH25, PER43, LH17) have isotope compositions similar to those collected from two wells (LH46 and LH46bis) located inside the caldera (≈2760 m.a.s.l.), in the producing area. This suggests a strong regionalization of the meteoric component.

Data from geothermal wells are from Arellano et al. (2003), Tello et al. (1990) and from the CFE database. All data refers to the total discharge composition and is thus recalculated based on discharge enthalpy (Henley et al., 1984). The geothermal well waters of the LHGF plot to the right of the meteoric lines and cover a very wide range of isotope values (about 10‰ and 40‰ for $\delta^{18}O$ and δD, respectively). When observed in more detail, many well waters are found to plot in a smaller area (about 5‰ and 15‰ of the $\delta^{18}O$ and δD ranges, respectively), and are mainly parallel to the abscissa. This pattern is typical for hot fluids in many geothermal fields worldwide (Craig, 1963; Truesdell and Hulston, 1980) and it is chiefly due to the isotope (mainly $\delta^{18}O$) shift taking place during the water-rock interaction under high temperature conditions. Due to the scattering of the points within and around the main group, secondary processes may affect the isotope signature of the LH geothermal well waters. Possible factors include: 1) boiling and steam separation, 2) influence of the isotopically fractionated re-injection fluid, 3) fluid extraction from different productive layers, 4) contribution by magmatic-volcanic deep fluids, 5) partial condensation at shallow levels, 6) interaction with CO_2. The commercial utilization of the LHGF since 1982 has enhanced the phase separation process, favoring conditions of excess of enthalpy and wellhead pressure drop, as documented by the production data of various geothermal wells (Arellano et al., 2015). The strong enrichment of heavy isotopes in fluids from re-injection wells sampled in this work (2017 and 2018) compared to those sampled in 1987 (Fig. 6) also provides evidence of the role played by this secondary process.

To establish the origin of the LH geothermal fluids and identify their possible feeding zones, the relationship between stable isotope ratios and altitude was investigated during the two years of observation. The $\delta^{18}O$ and δD values for water from small perennial springs located at different altitudes and at various lithologies were selected and plotted against the mean altitude of infiltration (estimated by a TDEM model taking into account the local morphology and geological conditions – see Fig. 7a-b). Spring waters located on the east sector of the LHGF (e.g. the Cofre de Perote volcano) show a different relationship of the isotope ratios with the mean infiltration altitude as compared to those of the spring waters located in the western sector (e.g. limestone outcrops on the Sierra Madre Oriental – see Fig. 7).

This feature was outlined for the first time in LH and was evident in both sampling trips (2017 and 2018). The evolution of different air masses and/or the isotopic fractionation process affecting the air masses during the crossing from upwind to downwind areas of local higher mountains (e.g. the Cofre de Perote volcano) account for this. In the east sector, the springs cover a wide range of altitudes (≈1950 m), but in the west sector where limestone outcrops are widely distributed, suitable springs are only located in a narrow range of altitude (≈250 m). The karstification of the limestone regional aquifers of the Sierra Madre Oriental (Issar et al., 1984) explains why small springs are seldom found and/or located at similar range of altitude. However, the isotope composition of the two well waters (LH46 and LH46bis) located at a high altitude inside the LH caldera can be inserted and used as a reference for the local meteoric component, as the difference between the altitude of the wells located at ground level and local morphological highs is quite small (<200 m). In both cases, the R-squared coefficient of the relationship between the isotope ratio and the mean altitude is >0.78, providing a value of 0.98 for the eastern relationship.

In order to better characterize local infiltration waters and identify possible rapid water circuits, some tritium analysis was also performed. Cold spring waters PER14 and PER69, both characterized by very low electrical conductivities (<60μS/cm) and low flow rates (<1 L/min.), show tritium activity respectively of 1.5 ± 0.6 TU and 1.4 ± 0.4 TU. These two springs are located close to the top of the local higher altitude (i.e. Cofre de Perote for the PER14 and Las Minas slope for the PER69) and they can be considered as an expression of local modern infiltration. Their tritium activities are in fact in agreement with those for modern precipitations at similar latitude (http://www-naweb.iaea.org/napc/ih/IHS_resources_isohis.html).

Tritium activities is 0.2 TU (±0.7 TU) in the water from a well close to the Los Humeros country (LH46) and 0.3 TU (±0.5 TU) in that from one of the warm wells located in the Perote plain (LH55). Although the uncertainties in tritium determination, it seems that waters from wells LH46 and LH55 may have basically lower activities than that for the local modern infiltration. The well LH46 is located at a high elevation (≈2800 m.a.s.l.) inside the Los Potreros caldera (see Fig. 2), very close to

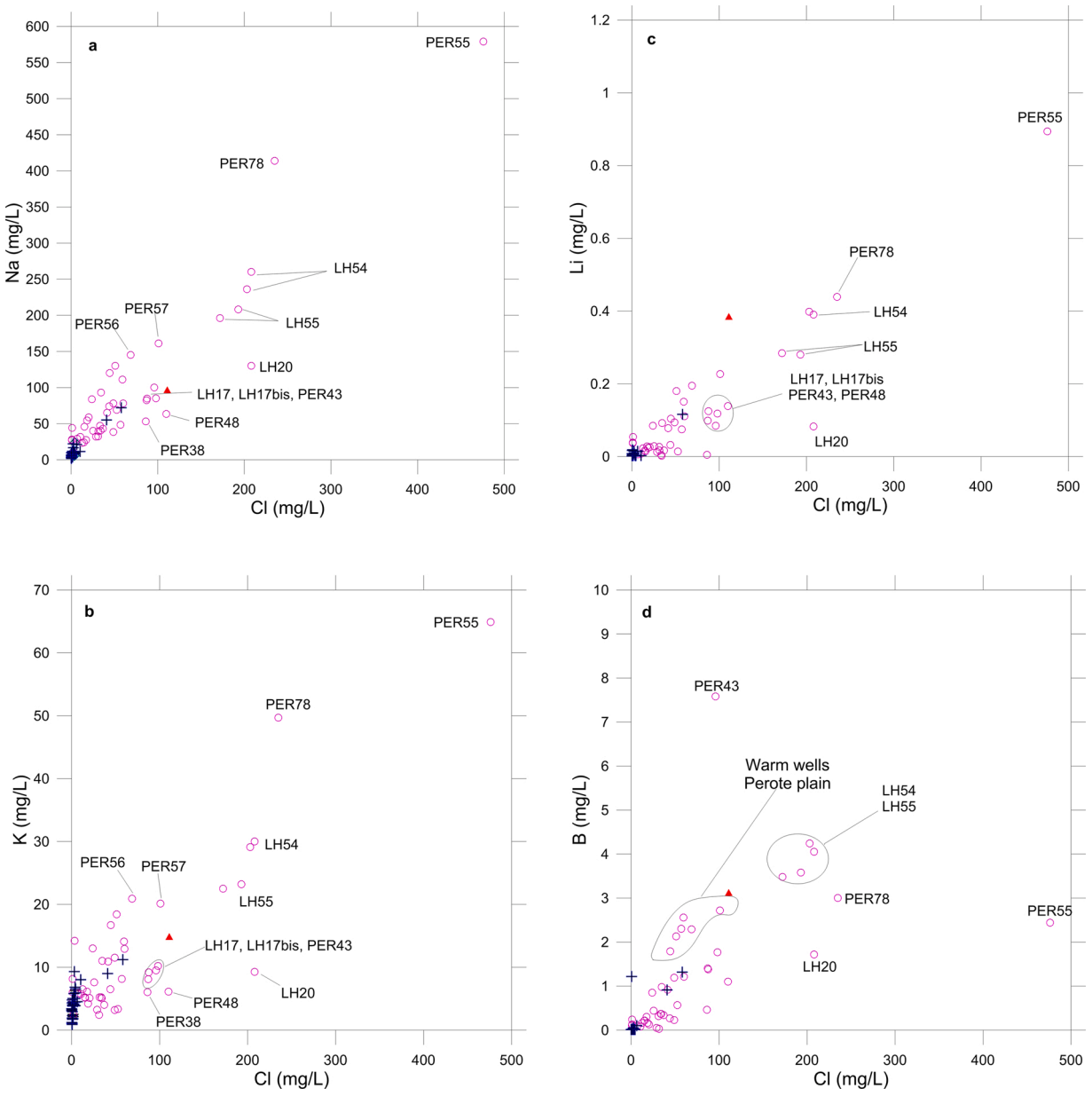

Fig. 5. Binary plots for dissolved species in water samples collected. (a) Na vs Cl; (b) K vs Cl; (c) Li vs Cl; (d) B vs Cl. Symbols as in Figure 3a.

the local higher altitude identified by the caldera rim (≈3000 m.a.s.l.). Therefore, assuming the rim of the Los Potreros caldera as a local watershed for this sample, its tritium activity could be an expression of a slow water circuit (i.e. low permeability conditions). On the contrary, taking into account the location of well LH55, the very low tritium activity might be associated with a long water circuit, as an expression of a regional meteoric component. However, taken into account the uncertainties in tritium determinations (especially for very low tritium activities), these hypotheses need to be clarified by further investigations.

4.2. Natural gas emissions

4.2.1. Chemical features

On a water-free basis, CO_2, N_2 and H_2S are the most abundant species present in the natural gas manifestations (Table 4 – Supplementary material). After considering all constituents, H_2O predominates (≥99 %) in fumaroles (i.e. LB1 sample).

The triangular diagram of CO_2–N_2–Ar (Fig. 8a) shows that all samples plot inside the compositional triangle of mantle-air-air saturated water (asw), suggesting mixing between these three components. Sample XA1 is most shifted towards a CO_2-rich component. The same path is also shown for most of the gas phases collected from geothermal wells, and no clear correlation with the geographical location of wells appears to be evident. In the triangular diagram CH_4–CO_2–N_2, the gas samples from Loma Blanca plot along the CO_2–N_2 axis, whereas the Xalapazco sample (XA1) plots close to the CH_4 vertex (Fig. 8b). This suggests that a redox transformation possibly took place at a shallow level, although other processes, such as magmatic degassing and thermal decomposition of organic matter can explain the production or addition of CH_4 in hydrothermal gases (Schoell, 1980, 1988; De Marais et al., 1988; Poreda et al., 1992; D'Alessandro et al., 2009). Geothermal well fluids are in generally plot along the CH_4–CO_2 axis, even if some located in the northern sector and characterized by shallower permeable horizons (<2000 m.a.s.l.) are shifted toward the N_2 vertex. The ternary diagrams of Fig. 8a and 8b show that the fumarole samples (i.e. LB1) have a similar chemical composition as those from the geothermal wells (i.e. H43 and H59) located in the northern sector of the producing area,

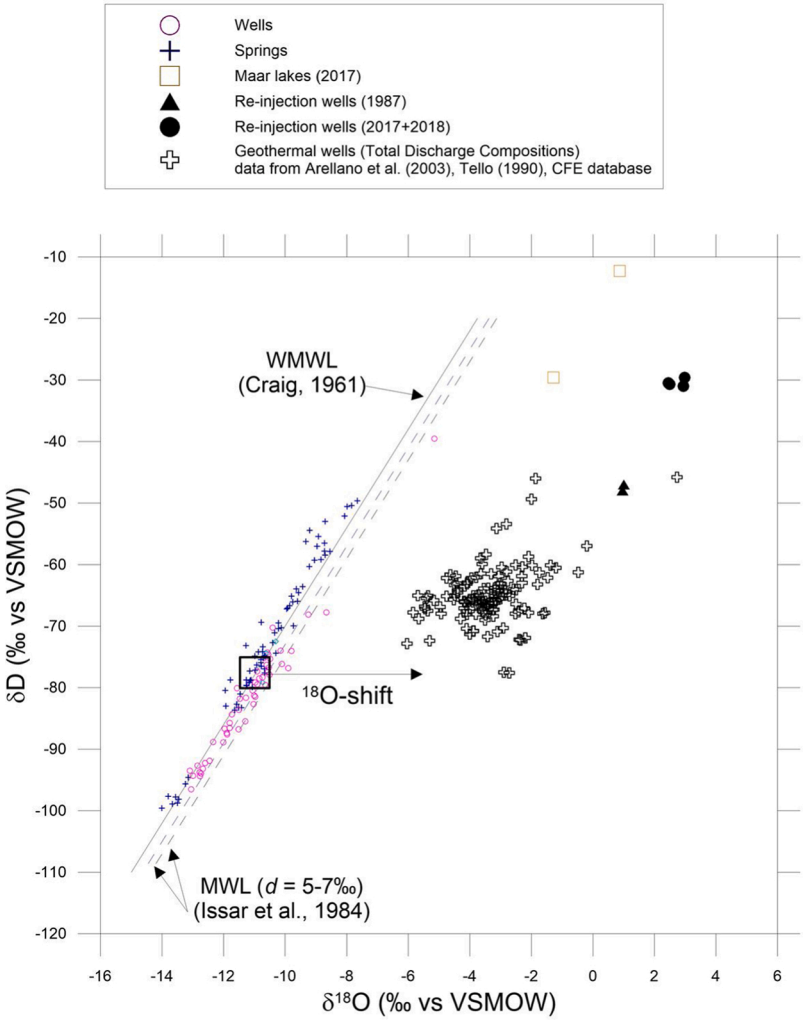

Fig. 6. Correlation plot δD‰ vs δ^{18}O‰ for water samples collected.

close to these natural manifestations.

CO, CH_4 and H_2 represent reactive species less affected by steam separation (due to the low solubility in the aqueous solution, Chiodini et al., 1992) and good geo-indicators for P-T-redox conditions, so inspecting the triangular diagram CH_4−CO−H_2 (Fig. 9) is beneficial. When approaching the CH_4-vertex, the natural gas manifestations in LHGF show typical characteristics of hydrothermal-geothermal gases, suggesting a hydrothermal origin (Chiodini et al., 1993).

As the natural gas manifestations in LHGF are sampled for a first time, it is interesting and useful to calculate the temperature of the liquid phase in equilibrium at depth (just for sample LB1, since it is less affected by air contamination and its temperature is very close to the boiling point, maintaining its gas/steam ratio). Following the suggestions provided by Chiodini and Marini (1998), the system independent of redox conditions was adopted. This approach considers the following two chemical reactions independent of the redox potential:

$$CO_2 + H_2 = CO + H_2O \quad (1)$$

$$3CO_2 + CH_4 = 4CO + 2H_2O \quad (2)$$

Their equilibrium constant expressions are:

$$logK_{(1)} = log\left(\frac{X_{CO}}{X_{CO2}}\right) - log\left(\frac{X_{H2}}{X_{H2O}}\right)$$

$$logK_{(2)} = 3log\left(\frac{X_{CO}}{X_{CO2}}\right) + log\left(\frac{X_{CO}}{X_{CH4}}\right) + 2logX_{H2O}$$

in which the use of ratios of molar fraction in the vapor phase (X_i) introduce negligible errors (Giggenbach, 1987), as the ratios of fugacity coefficients do not deviate significantly from 1 in the typical P,T range of hydrothermal systems, 100–374 °C and 1–220 bar (Ryzhenko and Volkov, 1971; Ryzhenko and Malinin, 1971; Naumov et al., 1974), for gas phases largely composed of water vapor (H_{H2O}>0.8).

The temperature dependence of the thermodynamic constants for reactions (1) and (2) are:

$$logK_{(1)} = -\frac{2248}{T} + 2.485$$

$$logK_{(2)} = -\frac{17813}{T} + 19.605$$

Following the approach by Chiodini and Marini (1998), the fumarole LB1 is possibly fed by a liquid phase at initial temperature of $T_0 = 291 \pm 5$ °C. This estimation is in agreement with those performed using different geothermometric techniques: $T_{H2/Ar}$ and $T_{CO2/Ar} \approx 270-338$ °C (Tello et al., 2005), $T_{Na/K} \approx 263-278$ °C (Tello, 1990), $T_{Na/K} \approx 290$ °C (Arellano et al., 2003) and $T_{FT\text{-}HSH2} \approx 228-330$ °C (Arellano et al., 2003).

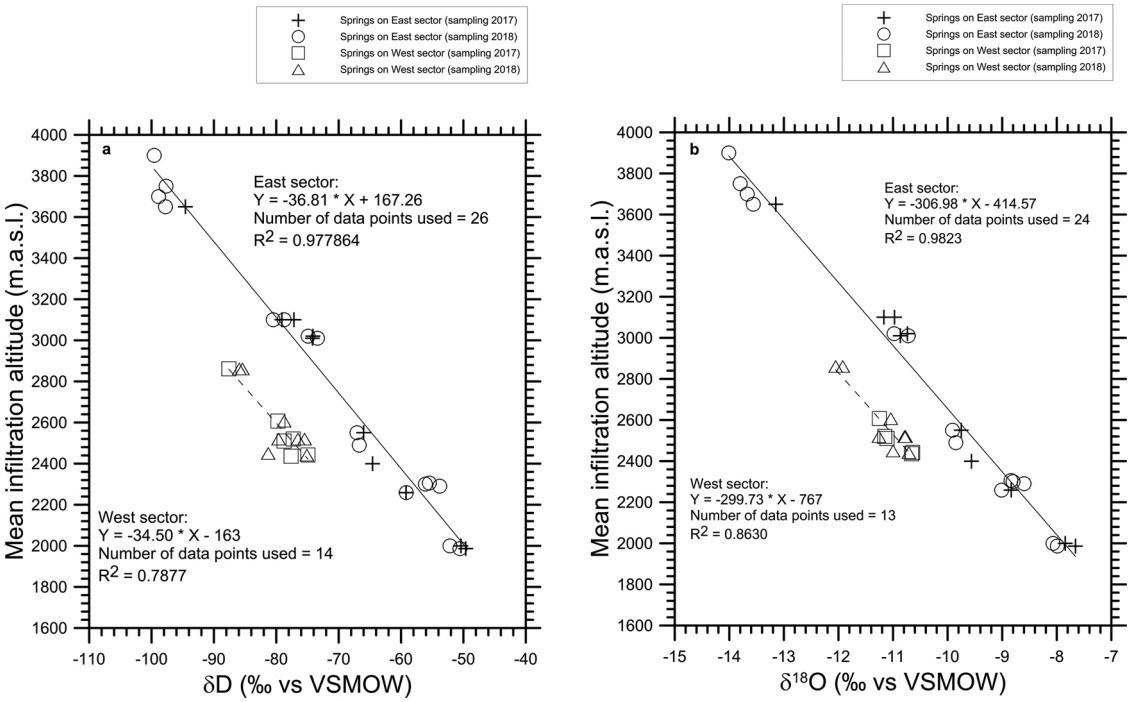

Fig. 7. Correlation of mean infiltration altitude with stable isotopic composition of water samples collected. (a) δD‰ vs mean infiltration altitude; (b) δ^{18}O‰ vs mean infiltration altitude.

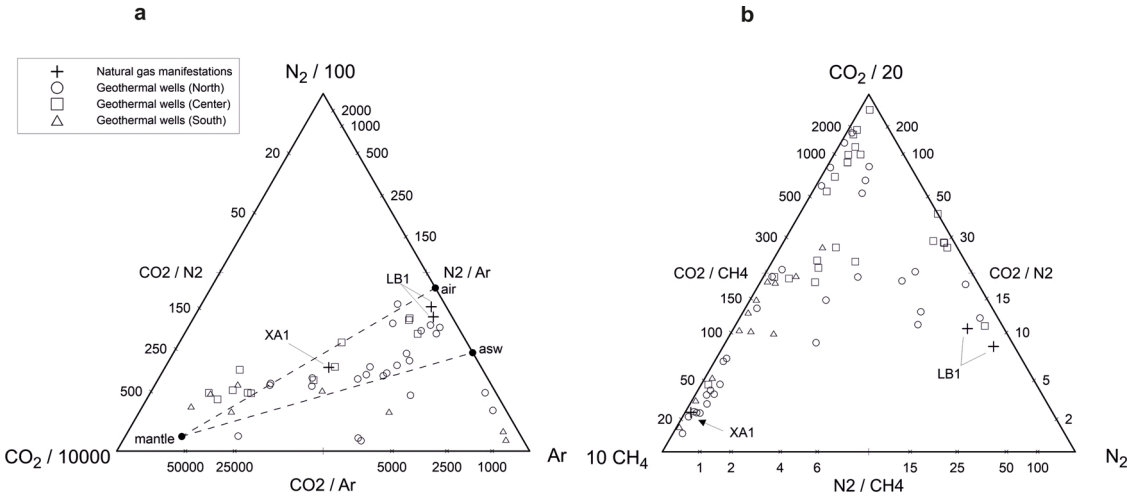

Fig. 8. Triangular diagrams for gas samples collected from natural manifestations: (a) CO_2-N_2-Ar diagram (modified after Giggenbach, 1997); (b) CH_4–CO_2–N_2 diagram. Geothermal well gases are also included for reference (data from Arellano et al., 2003; Tello et al., 2005; CFE).

4.2.2. Helium and carbon isotopes

Helium and carbon isotopes are of interest, as they represent sensitive tracers for fluids from mantle or magmatic sources, respectively, and for the thermo-metamorphism of carbonate rocks or from surface sediments (e.g. Sano and Wakita, 1985; Poreda and Craig, 1989; Giggenbach et al., 1993; Giggenbach and Poreda, 1993).

The $^4He/^{20}Ne$ ratios (Fig.10) are in the range of 2.6–30 and are thus higher than the air/ASW values (>0.28) and clearly indicate a He excess in all the collected samples. The presence of a deep-seated He derived from a ^{3}He-enriched source in all samples is unequivocally indicated by $^3He/^4He$ values between 1.4–3.3 Ra (with $R_a = {}^3He/{}^4He$ reference value for the air). The lowest $(R/R_a)_c$ values of 1.4, after atmospheric correction, are observed for fumarolic gases and can only be explained by the presence of additional radiogenic ^{4}He. A similar process was suggested for Los Azufres fluids (Pinti et al., 2013). Samples from geothermal wells show a wide range of $^4He/^{20}Ne$ ratios, but they show the same high R/R_a values. This pattern can be explained in terms of the simple mixing of the deep mantle component ($R/R_a \approx 7-8$) and air and/or asw. The fumarole samples plot away from the binary mixing curve connecting the mantle and the atmospheric components. As the atmospheric component is obviously presents and indicated by measurable amounts of $O_{2(g)}$ in the gases sampled (ranging between 47.5 and 80 ppmv - see Table 3 in the supplementary material), a possible ternary mixing between crustal, mantle, and atmospheric end-members is suggested (Fig.10).

The R/R_a values for the fumarole gases collected are plotted against their $\delta^{13}C-CO_2$ values (Fig. 11), following the approach of Richard et al. (2019). The dashed lines represent mixing hyperbolas (Langmuir et al., 1978) calculated for a mixture of mantle C and He ($R/R_a = 8 \pm 1$ and $\delta^{13}C-CO_2$ of -6 ± 2‰) and two distinct sedimentary sources: 1) organic

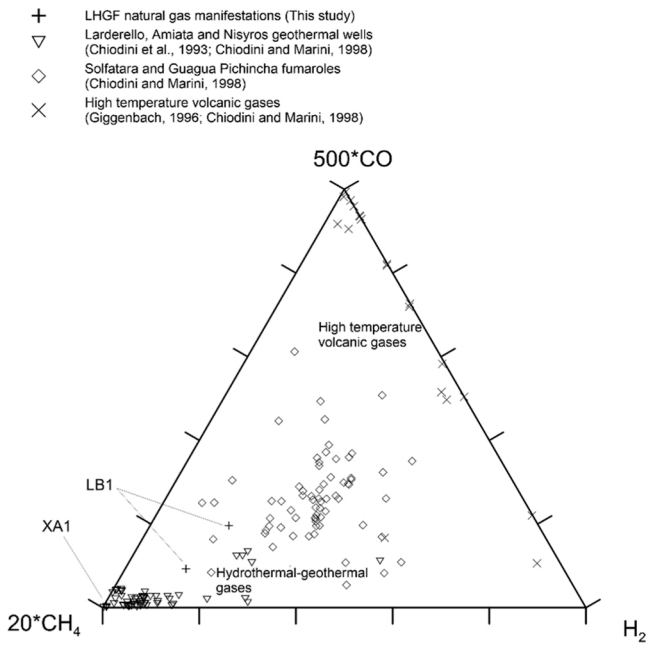

Fig. 9. Triangular diagram CH_4–CO–H_2 for gas samples collected from natural manifestations. Data from different kind of volcanic/geothermal systems are also included for reference (Chiodini et al., 1993 – modified).

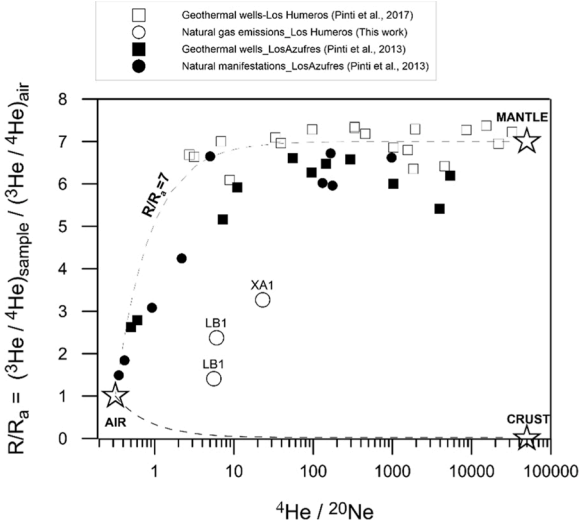

Fig. 10. R/R_a vs $^4He/^{20}Ne$ correlation diagram for gas samples collected from natural manifestations in LHGF. The air-mantle and air-crust binary lines are also shown. Data from LHGF geothermal wells and from Los Azufres geothermal system (wells and natural manifestations) are shown for comparison.

matter-rich sediment ($R/R_a = 0.02$ and $\delta^{13}C–CO_2$ of -20‰±10‰; Sano and Marty, 1995; Richard et al., 2019) and 2) carbonates ($R/R_a = 0.02$ and $\delta^{13}C–CO_2$ of 0‰±2‰; Pinti and Marty, 1998; Sano and Marty, 1995). From the $\delta^{13}C–CO_2$ values for the fluids from the LH geothermal wells, Richard et al. (2019) hypothesized, as did González-Partida et al. (1993) and Peiffer et al. (2018), a possible dissolution of the meta carbonates controlling the composition of the basement of the reservoir. The fumarole samples show the same range of variation in $\delta^{13}C–CO_2$, so a possible source of the CO_2 in the natural gas manifestations can be identified in the same meta carbonates. Compared to sample LB1, the depletion in the carbon isotope signature for CO_2 and the relatively high CH_4 concentration in sample XA1 suggests a possible redox transformation, at least at shallow levels. The carbon isotope composition for

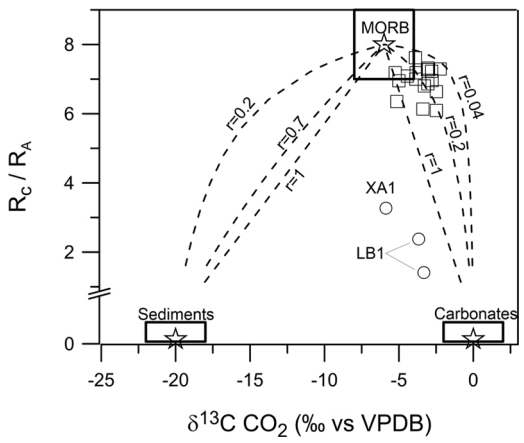

Fig. 11. Correlation diagram R_c/R_a vs $\delta^{13}C–CO_2$ for gas samples collected from natural manifestations in LHGF (modified after Richard et al., 2019). Data from geothermal wells of LHGF are also included. Symbols as in Fig. 10. Labels "r" are the curvature factors of the binary mixed trends, as given by the ratios of the CO_2/He quotient of the two components considered (i.e., $(CO_2/He)_{MANTLE}/(CO_2/He)_{SEDIMENT}$ and $(CO_2/He)_{MANTLE}/(CO_2/He)_{CARBONATE}$).

CO_2 and CH_4 in the sample XA1 ($\delta^{13}C–CO_2$ = -5.87‰ vs. VPDB; $\delta^{13}C–CH_4$ = -26.1‰ vs. VPDB) is generally in the typical range for geothermal gases (-9‰ $<\delta^{13}C–CO_2<$ -2‰; -30‰ $<\delta^{13}C–CH_4<$ -24‰, Craig, 1953, 1963; Hulston and McCabe, 1962a, 1962b; Ferrara et al., 1963; Gunter and Musgrave, 1971; Lyon and Hulston, 1984; Welhan, 1988). However, a contribution of CO_2 from a deep source is also possible.

To better understand the origin of gases from natural manifestations, combining information about isotopes and chemistry for the most abundant gas component (i.e. CO_2) is useful. In the diagram in Fig. 12, results for samples collected from natural gas manifestations in Los Humeros are reported together with a typical range of values for mantle, carbonate and sediment sources. The theoretical evolution of the binary mixing of a mantle end-member with carbonate or sediment end-members is shown by dashed lines. The fractions of each end-member are also reported. Gas samples collected in the LHGF plot inside the compositional area of sediments-mantle-carbonates, approaching the binary mixing line of mantle-carbonates and suggesting a high fraction of carbonate end-members (close to 0.9). Therefore, the observations of Figs. 11 and 12 suggest that in the LHGF the carbonate basement plays a pivotal role in defining the origin and evolution of geothermal fluids and feeding the natural gas manifestations.

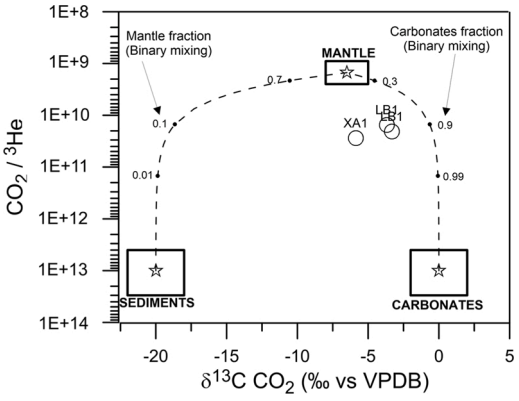

Fig. 12. Correlation diagram $CO_2/^3He$ vs $\delta^{13}C–CO_2$ for gas samples collected from natural manifestations in LHGF (modified after Sano and Marty, 1995). By applying a three components mass balance approach, we estimate the following relative Mantle (MORB)-Sediments-Carbonates proportions (%): LB1 8.6-15.8-75.6; LB1 8.1-14.2-77.7; XA1 5.6-27.7-66.7.

5. Geochemical modeling

An important task in geothermal fluid geochemistry is to provide data and information on the geochemical conceptual model of the studied system, as this is an essential tool for further exploration activities and/or production planes.

In a generic model of a geothermal system local meteoric water can infiltrate and be heated at depth, reacting with host/reservoir rocks and then rising to the surface after boiling and phase separation, in the form of thermal springs, bubbling springs, fumaroles and/or steaming ground. At depth, the meteoric component can also be mixed with magmatic-volcanic components released by the magma body (Taylor, 1971; Henley and Ellis, 1983; Hedenquist, 1986; Giggenbach, 1987, 1992b; Hedenquist and Lowenstein, 1994).

Water-rock interaction and steam separation were considered as explanations for the processes regulating the isotope composition of the geothermal fluids and fumarolic discharges in Loma Blanca. Thus, it is useful to plot the δD and $\delta^{18}O$ values for geothermal fluids and steam discharges, together with those for cold meteoric waters and possible interacting rocks (Figs. 13a and b).

Geochemical modeling was used to identify the isotope composition of possible infiltrating meteoric water (IW) and deep water (DW) based on observed experimental data. As postulated in previous works (Truesdell et al., 1977; Giggenbach, 1978; Giggenbach and Stewart, 1982), the Single Step Vapor Separation (SSVS) reproduces the natural steam separation effectively. Thus, following the approach of Giggenbach and Stewart (1982), the relationships for calculating the isotope composition of the liquid δ_w and vapor phase δ_s after the SSVS process were obtained (the mathematical derivation is discussed in the appendix A.1):

$$\delta_w = \delta_0 + \varepsilon y_s \quad (3)$$

$$\delta_s = \delta_0 - \varepsilon(1 - y_s) \quad (4)$$

where y_s and ε are the steam fraction and fractionation factor, respectively.

The results from Eqs. (3) and (4) can be plotted in the binary diagram δD‰ vs $\delta^{18}O$‰ (Fig. 13a), as *primary water after SSVS* and *primary steam from DW (Deep Water)* curves, respectively. The best fit with the isotope composition of the fumarole sampled is obtained for a hypothetical DW with a temperature of 291 °C (estimate based on the sum of the log-ratio of H_2/H_2O, CO/CO_2 and CH_4/CO_2 – see Chapter 4.2.1.) and an isotope composition of about δD_{DW} = -76.0‰ and $\delta^{18}O$= -4.35‰. The DW composition generally represents the result of the interaction between the meteoric component and rocks at high temperature (i.e. an 18-oxygen shift). The fractionation induced by this process can vary considerably, as the reaction progress of the water-rock interaction process represents a variable that is unknown *a-priori*. However, by considering a $\Delta^{18}O$ of about ±1‰, the hypothetical range of values for the isotope composition of the DW is δD_{DW}‰ = -76.0 ± 0.4; $\delta^{18}O_{DW}$ = -4.35‰±1. In Fig. 13a, the range of values for the DW enables a theoretical set of curves parallel to that for the *primary water after SSVS* and to that for the *primary steam from DW* (see solid curves in Fig. 13a). The different fractions of separated steam (y_s) are also reported. These grids can reproduce the isotope composition for several liquids from the geothermal wells and also for the condensed steam from the natural gas manifestation collected. Similar results can be also obtained by modeling the fractionation of stable isotopes as a Continuous Steam Separation (CSS), by means of Rayleigh distillation (Fig. 13b):

$$\delta R = \delta_{R(0)} - 1000*[f^{(\alpha-1)}-1] \quad (5)$$

in which δR is the final isotope composition in the delta notation of one of the two phases, $\delta R_{(0)}$ is the initial isotope composition in the fluid, *f* is the liquid fraction for liquid or vapor (Horita and Wesolowski, 1994), and α is the fractionation factor. Beginning with the DW, the evolution of the stable isotope composition of geothermal liquids is reported in Fig. 13b for fractions of residual liquids of 0.1, 0.3 and 0.5. In addition to the evolution of stable isotopes for geothermal liquids, the Rayleigh distillation is also consistent with the isotope composition of condensed

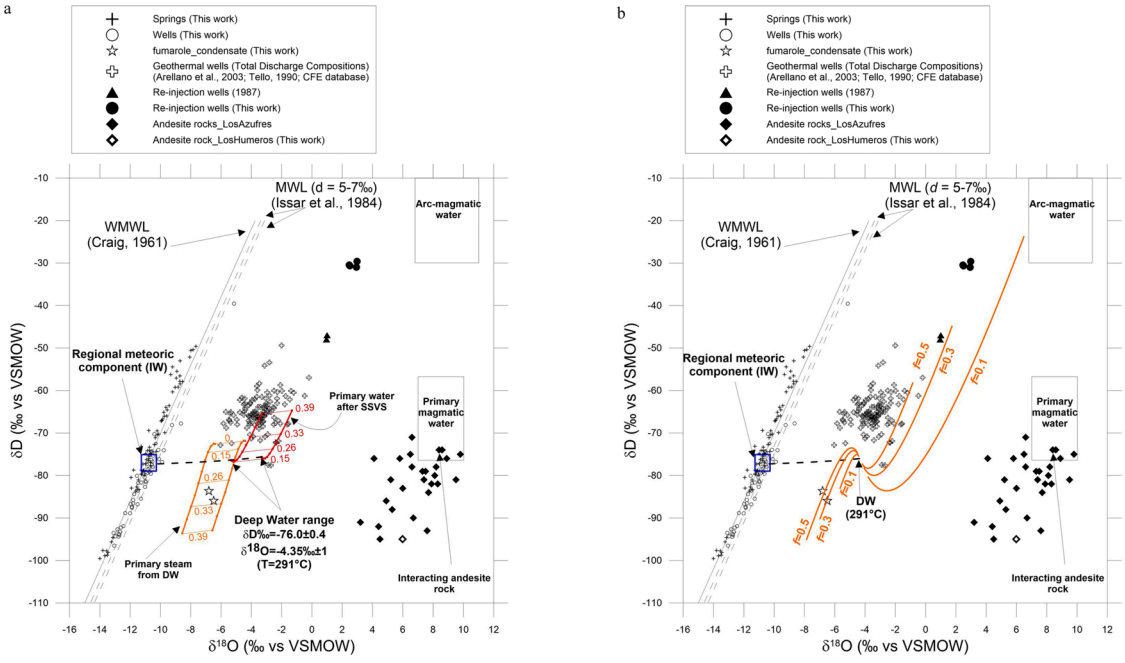

Fig. 13. (a) Correlation diagram δD‰ vs $\delta^{18}O$‰ in which experimental data for geothermal and cold fluids are compared to the theoretical stable isotope composition of primary steam from Deep Water (DW) and primary water after Single Step Vapor Separation (SSVS) process (represented by solid curves). Fractions of separated steam (y_s – i.e. numbers close to solid lines) and the range of variation of isotope composition for the hypothetical Deep Water (DW) are also reported. (b) Correlation diagram δD‰ vs $\delta^{18}O$‰ in which experimental data for geothermal and cold fluids are compared to the theoretical fractionation of stable isotopes, for the hypothetical Deep Water (DW) and obtained separated Steam water under Continuous Steam Separation process (CSS – solid curves). For simplicity, the continuous steam separation curves were reported only for a single value of the isotope composition for the DW (i.e. δD_{DW} = -76.0‰ and $\delta^{18}O$ = -4.35‰).

steam determined in the fumarole fluid of Loma Blanca.

The isotope composition estimated for the DW is then used as a constraint for the water-rock isotope exchange model described in Appendix A.2. As the main geothermal producing levels are located in andesite rocks, the model considers that geothermal fluids prevalently interact at high temperatures with this type of rock. The stable isotope composition reported by Torres-Alvarado et al. (2012) were used, as they represent examples of less-altered Mexican andesites. Our model also assumes the mass conservation of the isotopes in the whole rock-fluid system under conditions of a multi-phase isotopic equilibrium. As shown in Figs. 13a and b (see the dashed lines), the results of the model match the composition of the hypothetical DW, assuming that infiltrating meteoric waters (IW) have an average initial isotope composition of δD_{IW} = -77.3‰ and $\delta^{18}O_{IW}$ = -10.50‰. This isotopic composition is in good agreement with the average value obtained from most of the cold springs (LH5, LH6, LH7, LH8, LH8bis, LH14, PER84, PER85 - δD = -77.5‰ and $\delta^{18}O_{IW}$ = -10.89‰) located in the limestone outcrops of the Sierra Madre Oriental (on the west sector of the LHGF – Fig. 2). A small cluster of springs (LH23, LH24, LH26 and LH27) located in volcanic rocks in the south-eastern side of the studied area can also be considered consistent with the results of the model. However, based on their stable isotope composition and locations, it appears that these springs feed the surface cold aquifer developed in the adjacent plain, in which several water wells are drilled (e.g. PER47, PER48, PER49 – see Fig. 2). This can also be assumed for wells located in the Perote plain (PER11, PER26 and PER57), as their waters represent a mixing of the most depleted meteoric components from the Cofre de Perote volcano (represented by springs LH35, LH36, LH37, PER13, PER14 and PER15) and local infiltration at lower altitudes (e.g. PER67, PER68, PER69, PER70).

To verify the presence of possible feeding zones located inside the Los Potreros caldera, the same model was used to simulate the interaction of andesite rock with a hypothetical IW with an isotope composition similar to that determined in the two well waters LH46 and LH46bis,

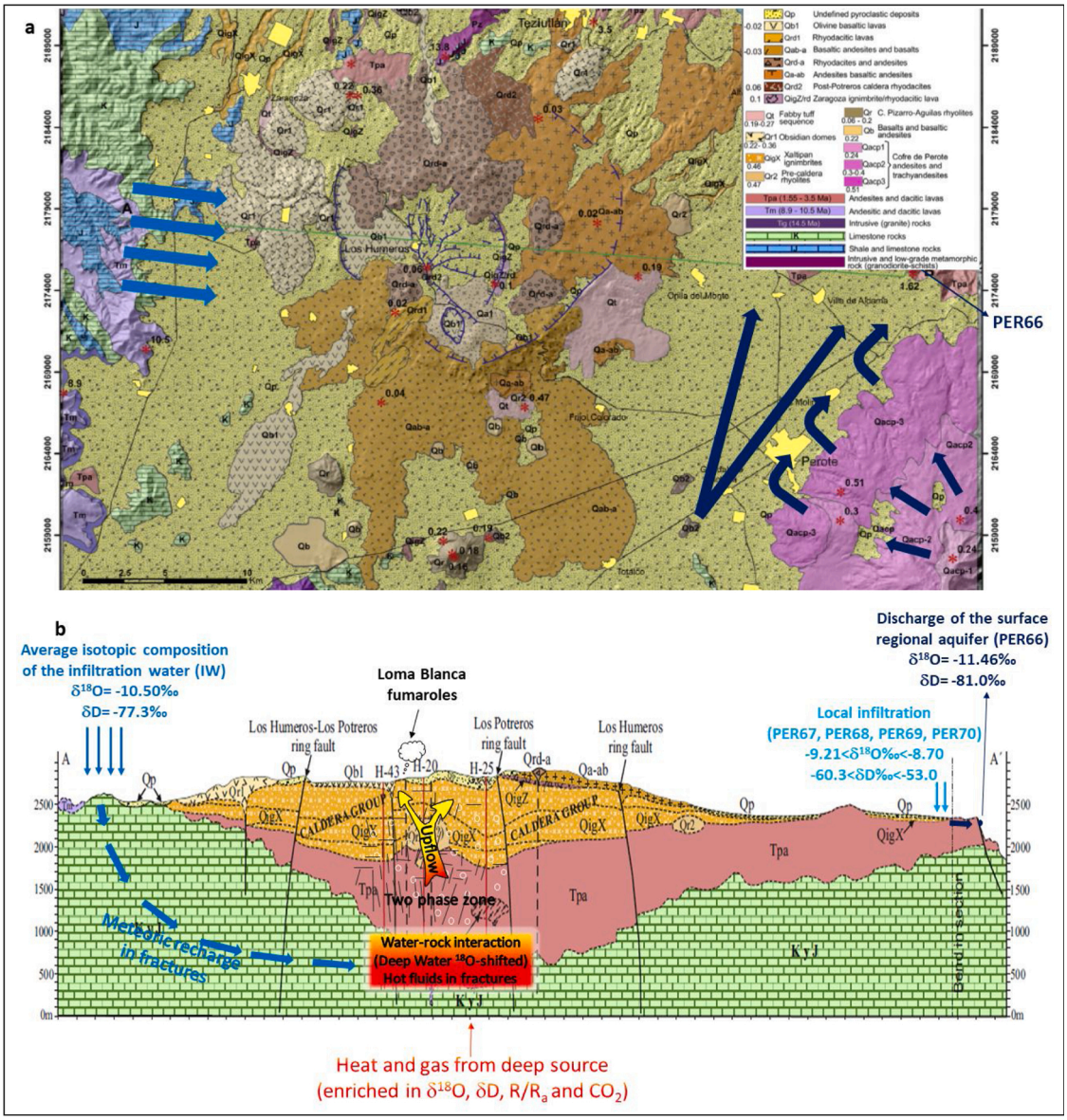

Fig. 14. Schematic conceptual model for the LHGF. The geological map and the cross section are from Carrasco et al., 2017a (modified). a) Sketch map of the possible fluid flow-path. Light blue arrows represent the meteoric component, which can be involved in the feeding of the LHGF. Dark blue arrows represent the flow-path of the shallow regional aquifer present in the Perote plain and one of its main feeding zones (i.e. the Cofre de Perote volcano). b) Cross section in which the isotope composition of hypothetical DW and IW are reported, together with possible source end-members and fluid flow-paths. The discharge of the surface regional aquifer in the Perote plain is also reported. The vertical axis is exaggerated.

which are at high altitudes (~2800 m.a.s.l.) inside the caldera. Although the isotope composition of the condensed steam collected from fumaroles is also reproduced for this simulation, the theoretical evolution of the primary water matches the isotope composition of the liquids discharged by geothermal wells at extremely low separation temperatures (<100 °C, and thus with no physical meaning).

6. A conceptual model proposed for LHGF

A schematic conceptual model for the LHGF is reported in Fig. 14, which represents an attempt to identify the mean feeding zones, the possible end-members involved and the fluid flow-path. The main feeding zones are located in limestone outcrops of the Sierra Madre Oriental, on the western side of the LHGF. This component, identified as IW and representing the regional meteoric component (δD_{IW} = -77.3‰ and $\delta^{18}O_{IW}$ = -10.50‰), seeps and goes down into the limestone formation, approaching the contact with andesite rocks. It is worth noting that infiltration and deepening of a meteoric component may occur in limestone formations where fractures guarantee sufficient permeability and transmissivity. As in all fractured media, the permeability has to be considered compartmentalized in separated sectors or units, some of them permeable and other practically impervious. However, on a regional scale, the karstification of limestone aquifers and the presence of caves (Issar et al., 1984) may favor the infiltration process. At depth, the interaction at high temperatures between IW and andesite rocks promotes the ^{18}O-shift and produces the DW (δD_{DW} ‰ = -76.0 ± 0.4; $\delta^{18}O_{DW}$ = -4.35‰±1). Loma Blanca fumarole fluids may originate in a phase separation process (e.g. SSVS or CSS), starting from the hypothesized DW at an initial temperature of about 290 °C. The results obtained from the proposed models are in good agreement with the experimental data for the natural gas emissions in Loma Blanca. The data for many of the geothermal liquids discharged by geothermal wells are also consistent with the results of the models, even if the agreement cannot be considered satisfactory for all the experimental data. This suggests that SSVS or CSS cannot be considered as the only possible phase separation processes active in LHGF, and the distribution/-fractionation of water stable isotopes in geothermal liquids is probably the result of the sum of the effects. As most of the producing wells (excluding wells H-1 and H-49) are characterized by excess enthalpy conditions (i.e. a two-phase mixture directly present in the geothermal reservoir), a phase segregation process can also be considered (Arnórsson et al., 2007; Pope et al., 2016). Based on this process, liquid water is completely or partially adsorbed onto mineral grain surfaces due to various capillary forces, and will be separated from the vapor phase during the transport through the geothermal reservoir and into the producing wells (Gudmundsson and Arnórsson, 2002; Giroud, 2008; Angcoy, 2010; Karingithi et al., 2010). Thus, phase segregation is a complex process and its effect on the geochemistry of geothermal fluids discharged by geothermal wells may be different in different wells. Unfortunately, as all the data required is not available (i.e., the chemistry of geothermal liquids and the vapor and stable isotope values for hydrous alteration minerals, Pope et al., 2016), the evaluation of the effect of phase segregation remains qualitative in this work. Based on the data obtained, the presence of other possible processes cannot be ruled out: a) volcanic-magmatic deep fluids, even if their contribution appears to be smaller than previously believed (up to 10–15 %); b) re-injected fluid, although its influence appears to be limited to producing wells located close to re-injection wells; c) CO_2-steam exchange (D'Amore and Panichi, 1987; Clark and Fritz, 1997), as CO_2-rich gases are present in fluids from geothermal wells. Mixing of the IW with volcanic-magmatic deep fluids may take place before or after water-rock interaction and/or steam separation processes, with the isotope composition of a geothermal liquid discharged from a generic geothermal well being very similar to one obtained through a different order of the previous mentioned natural processes.

In addition, the chemical and isotope composition of well discharges, along with the fraction of separated vapor and gas, are likely modified by power production activity (i.e. due to the decrease in pressure induced by the withdrawal of fluid from a system), and the effect on the gas concentration depends on the well position and the duration of discharge (Giggenbach, 1980). All the processes and components mentioned above can contribute to the spread of geothermal liquid data in the plots of Fig. 13(a and b), and thus may be considered when interpreting the disagreement between the modelled and experimental data for some geothermal wells.

The isotope composition of the hypothetical IW was finally used to estimate the mean altitude of the infiltration areas. Using the relationship between *stable isotopes* and *altitude* reported in Figs. 7a and b, the mean infiltration altitude ranges are about 2400–2650 and 2850–3100 (m.a.s.l.) for the western and eastern sectors, respectively. The former range of altitudes is widespread in the Sierra Madre Oriental ridge and in some sector of the plain located between the Sierra Madre Oriental ridge and the LH producing area. The limestone outcrops extending in those areas may constitute a wide infiltration surface for the geothermal system. The presence and the distribution of fractures strongly affect the recharge of the deep system and, consequently, the rate and velocity of flow paths can vary considerably from one sector to another. The presence of long and/or slow water circuits leads to long residence time at depth, possibly explaining the relatively high radiogenic argon found in few geothermal wells (Pinti et al., 2017).

The importance of the meteoric component, and in particular of the regional component (from outside the Los Potreros and Los Humeros Calderas), is also suggested in terms of the water budget. The average rainfall in the Sierra Madre Oriental basin is at least three times that close to the Los Humeros area, inside the Los Potreros caldera (from the data of the National Meteorologic Service of Mexico, http://clicom-mex.cicese.mx/).

Water stable isotopes allow to confirm that the shallow volcanic aquifer developed in the Perote plain receives a contribution from the Cofre de Perote volcano (dark blue arrows in Fig. 14a), but other contributions from the southern part of the plain are also identified. Globally, the water flows in this shallow aquifer toward NE direction, as confirmed by the stable isotopic composition of water discharged by cold spring having a very high flow rate (PER66) and located close to the Las Minas area (see the eastern portion in Figs. 14a and b for location). Its isotope composition ($\delta^{18}O$= -11.46‰, δD= -81.0‰) is much lower than that of the water from small springs representing the local infiltration component (PER67, PER68, PER69, PER70 – which were collected close to the sample PER66). On the contrary, the sample PER66 shows similar characteristics to waters infiltrated at a higher altitude.

7. Conclusions

A detailed fluid geochemical survey has been performed in the Los Humeros area that provided new constraints for the hydrogeochemical model of the LHGF. In particular, the chemical and isotope composition of waters and gases support the regional recharge of the geothermal system, with groundwater recharge likely occurring on Sierra Madre Oriental mountainous range. The isotopic composition of the infiltration water (IW) and of the deep geothermal component (DW) have been defined based on the stable isotope composition of oxygen and hydrogen in water and gas samples, liquids from geothermal wells and local rocks (i.e. andesites), by taking into account the isotope fractionation effects associated with water-rock interactions and boiling/phase separation processes (SSVS and CSS).

Based on this conceptual model, fluid flow-paths towards the deep levels in the central sector of the geothermal system, are supposed to be originated in the limestone outcrops widely present on the west side of the LHGF (Sierra Madre Oriental ridge). The same limestones are also present at the bottom of the LH productive levels and, thus the meteoric component that can infiltrate in the Sierra Madre Oriental ridge may reach the roots of the LHGF or the deeper portion of the hot water

circulation. Faults and fractures (e.g., the Los Humeros ring-fault and the Maxtaloya fault, both aligned NNW-SSE in the west sector of the LHGF) cause the dislocation of rocks from different geological formations (e.g. limestones and volcanic rocks), thus promoting secondary permeability and the inflow of circulating water into the andesite reservoirs. Some uncertainties regarding the hydraulic connection between limestones and andesitic rocks remain, but the input of the regional meteoric component inside the super-hot portion of the LHGF is in agreement with the water stable isotope data, even if the inflow may be localised in some sectors. The meteoric component can interact with volcanic rocks at a high temperature, increasing its $\delta^{18}O$ values (an 18-oxygen shift). Geothermal well fluids from H-1 and H-49, characterized by no excess or less excess of enthalpy, demonstrate that the hot liquid phase can be present at depth also in a superhot geothermal system, such as the LHGF. Of course, the presence of a liquid phase in fractures depends on the local permeability conditions. Deep hot fluids undergo boiling and phase separation, upflowing to shallow levels and feeding the natural gas manifestations. This hypothesis is supported by the experimental data obtained and by the geochemical models proposed in this study (e.g. SSVS and CSS), although other processes must be considered when interpreting all the data for the fluid discharged by geothermal wells. In particular, a phase segregation, gas-exchange, re-injection of fluids and a possible input from magmatic-volcanic deep fluids cannot be ruled out, despite the low contribution of deep fluids (up to 10–15 %). The 35 years of power production represents a further complication when interpreting the evolution of the data available from geothermal wells, as this contributes to increases in the pressure drop and the vapor/liquid ratio. Despite the effects induced by various possible natural processes and by the power production activity, the conceptual model proposed agrees with the geochemical data and represents a good point of reference when investigating the origin and evolution of fluids in the LHGF, at least in overall terms. It is also consistent with the evidences from regional and local geology.

A number of geophysical and geological data was collected from the LHGF to identify and characterize the faults/structures responsible for the permeability of the reservoir and in the portion above. Although this data contributes to the knowledge of the LHGF, one important factor is the identification of the mechanism responsible for the input of the meteoric component in the super-hot portion of the LHGF. Thus, more details regarding the relationships and contact between limestones and andesites in zones located outside the LH producing area could be very useful. If this contact plays a pivotal role by regulating the input of the regional meteoric component, other investigations are required, as the availability of geothermal fluids and thus the planning of future production may depend on it.

Authors contributions

L.M. designed and drafted the manuscript with input from all of the authors, and with K.T. leaded the fieldworks. L.M., K.T., S.A.J., C.J. and D.M. participated in the fieldwork, and with M.G., G.F., N.F. reviewed the manuscript.

Declaration of Competing Interest

The authors report no declarations of interest.

Acknowledgements

This paper presents results of the GEMex Project, funded by the European Union's Horizon 2020 programme for Research and Innovation under grant agreement No 727550, and by the Mexican Energy Sustainability Fund CONACYT-SENER, Project 2015-04-268074. This work was also supported by the CeMie-Geo Consortium financed by SENER-CONACYT (No. 2007032). The Authors wish to thank the Comisión Federal de Electricidad (CFE) of Mexico for the access to the geothermal concession area and for useful meetings performed in the CFE headquarter in Los Humeros. Logs and physico-chemical parameters of geothermal wells and chemical and isotope data for several cold waters were also provided by CFE. Special thanks to the Universidad Michoacana San Nicolas Hidalgo (UMSNH), which provided support to rent vehicles for field trips. We acknowledge Sanjuan Bernard, Frederick Gal, Francisco del Toro, Eduardo Gonzales Manzano, Ruth Alfaro Cuevas Villanueva, Pedro Alfaro Cuevas Villanueva, Carlos Ramirez Gaytán, Julio Cesar Canas Ramirez, Yan Rene Ramos, Roberts Gamez Bocanegra and the CFE personnel for their valuable help and support during field work. We also acknowledge the GEMex team for useful discussion, and Chiara Boschi and Ilaria Baneschi for carbon isotope analyses. We wish to thank Associate Editor Dr. Halldór Ármannsson and two anonymous reviewers for their constructive comments and suggestions and Prof. Luigi Marini for very fruitful discussions.

Appendix A

A.1 Evaluation of steam separation process on the isotopic composition of the liquid δ_w and vapor phase δ_s

Following the approach used by Giggenbach and Stewart (1982), the isotope composition of separated steam (assuming Single-Step Vapor Separation, SSVS) and water was calculated by use of the isotope balance:

$$\delta_s y_s + \delta_w (1-y_s) = \delta_0 \quad \text{(a1)}$$

in which δ_0, δ_s, δ_w represent respectively the isotope composition of a single liquid-phase fluid before vapor separation (i.e. Deep Water in the reservoir - DW) and those of vapor and liquid phases after phase separation. The coefficient y_s is the steam fraction, which can be evaluated as follows:

$$y_s = \frac{(H_0 - H_w)}{(H_s - H_w)} \quad \text{(a2)}$$

where, H_0 H_s and H_w are the enthalpies of the liquid-phase fluid before separation and those of the steam and water phases at the temperature of vapor separation, respectively. Considering the distribution of deuterium and oxygen-18 between liquid and vapor phases as a process close to equilibrium (Giggenbach, 1971), the equilibrium constant (α) can be related to the fractionation factor (ε):

$$\varepsilon = 1000\, ln\alpha \cong 1000\,(\alpha - 1) \cong \delta_w - \delta_s \quad \text{(a3)}$$

Combining Eqs. (a1) and (a3), is it possible to obtain the relationships to calculate the isotope composition of the liquid δ_w and vapor phase δ_s, after SSVS, in function of y_s and ε:

$$\delta_w = \delta_0 + \varepsilon y_s \quad \text{(a4)}$$

$$\delta_s = \delta_0 - \varepsilon(1 - y_s) \quad \text{(a5)}$$

A.2 Evaluation of steam separation process on the isotope composition of the liquid δw and

A number of equations have been developed in the literature that describe a water-rock interaction process relying on the principle of the mass conservation of the isotopes in the whole rock + fluid system, under conditions of multi-phase isotope equilibrium (e.g., Taylor, 1977, 1979; Ohmoto, 1986). These models are an oversimplified representation of the complex processes expected to occur at depth, and major sources of uncertainty are associated with the intrinsically unknown spatial and temporal distribution of temperature, of the mineralogical composition of rocks, and of the initial isotope composition of both fluids and minerals throughout the (presumably large) rock volume affected by the water-rock alteration process. Moreover, the isotope fractionation factors between water and silicates under hydrothermal conditions are poorly known, in particular for hydrogen (Chacko et al., 2001). Despite these limitations, these models provide an adequate, though qualitative, representation of the natural processes underground (e.g., Taylor, 1979). In our model we assume that the oxygen and hydrogen stable isotope exchange between rocks and circulating fluids prevalently takes place through the hydrothermal conversion of primary silicates (e.g., plagioclase, feldspars) to layer silicates (e.g., micas), as symbolised by the following reaction (Giggenbach, 1993):

$$an + kfs + H_2O + CO_2 \rightarrow musc + 2SiO_2 + cc \quad \text{(a6)}$$

This model considers that rock alteration is predominantly driven by CO_2-induced acidity of fluids within the roots of the hydrothermal systems (Giggenbach, 1993). A reasonable fit between our theoretical curves and field data was obtained by assuming $\varepsilon^{18O}_{min-H2O}$ and $\varepsilon^{2H}_{min-H2O}$ values in the range 4 ± 0.5‰ and -25 ± 0.5‰, respectively, similar to the fractionation factors governing the equilibration of water with K-mica at 300 °C (Taylor, 1979).

Appendix B. Supplementary data

Supplementary material related to this article can be found, in the online version, at doi:https://doi.org/10.1016/j.geothermics.2020.101983.

References

Alcocer, J., Hammer, U.T., 1998. Saline lake ecosystems of Mexico. Aquat. Ecosyst. Health Manag. 1, 291–315.
Angcoy Jr., E.C., 2010. Geochemical Modeling of the High- Temperature Mahanagdong Geothermal Field, Leyte, Philippines. Master's thesis. University of Iceland, Reykjavik, Iceland, p. 126p.
Arellano, V.M., Garcia, A., Barragán, R.M., Izquierdo, G., Aragon, A., Nieva, D., Portugal, E., Torres, I., 1998. Desarrollo de un modelo basico actualizado del yacimiento de Los humeros, Puebla. Report IIE/11/11459/I01/F for the Comision Federal De Electricidad. Instituto de Investigaciones Electricas, Temixco, Mor, p. 450.
Arellano, V.M., García, A., Barragán Reyes, R.M., Izquierdo, G., Aragón, A., Nieva, D., 2003. An updated conceptual model of the Los Humeros geotermal reservoir (México). J. Volcanol. Geotherm. Res. 124, 67–88.
Arellano, V.M., Barragán, R.M., Ramírez, M., López, S., Paredes, A., Aragón, A., Tovar, R., 2015. The response to exploitation of the Los Humeros (Mexico) geothermal reservoir. In: Proceedings World Geothermal Congress. Melbourne, Australia, 19-25 April.
Arnórsson, S., Stefánsson, A., Bjarnason, J.O., 2007. Fluid-fluid interactions in geothermal systems. Rev. Mineral. Geochem. 65, 259–312.
Barragán, R.M., Santoyo, E., Nieva, D., Portugal, E., Verma, M.P., 1988. Caracterizacioin de yacimientos geotermicos mediante la determinacion de parametros fisico-quimicos. Internal Report IIE/11/2386/I 01/F. Instituto de Investigaciones Electricas, Temixco, Mor, p. 250.
Barragán, R.M., Cervantes, M., Diaz, R., Garduno, V., Gonzalez, E., Holgun, S., Meza, F., Nieva, D., Oliver, R., Rosas, N., Sampedro, J., 1989. Caracterizacioin del fenomeno de corrosion-obturacion en pozos de Los Humeros. Report IIE/11/3753/I for the Comision Federal De Electricidad. Instituto de Investigaciones Electricas, Temixco, Mor, p. 83.
Barragán, R.M., Nieva, D., Santoyo, E., Gonzalez, E., Verma, M., Lopez, J., 1991. Geoquimica de fuidos del campo geotermico de Los Humeros (Mexico). Geotermia Rev. Mex. Geoenerg. 7, 23–47.
Barragán, R.M., Portugal, E., Martínez, J., 1998. Estudio Isotopico De Fluidos De Pozos Productores Del Campo Geotermico De Los Humeros. Informe IIE/11/11173/I 02/F, Puebla, p. 45.
Barragán, R.M., Arellano, V.M., Armenta, M.F., Aguado, R.T., 2008. Cambios quimicos en fluidos de pozos del campo geotermico de Los Humeros: evidencia de recarga profunda. Geotermia 21 (2).
Barragán, R.M., Arellano Gomez, V.M., Ramírez Montes, M., Tovar Aguado, R., 2010. Geoquimica isotópica ($\delta^{18}O$, δD) inicial de fluidos de pozos del campo geotérmico de Los Humeros. Pue. Geotermia 23 (1), 16–25.
Carrasco-Núñez, G., Branney, M.J., 2005. Progressive assembly of a massive layer of ignimbrite with normal-to-reverse compositional zoning: the Zaragoza ignimbrite of central Mexico. Bull. Volcanol. 68, 3–20.
Carrasco-Núñez, G., McCurry, M., Branney, M.J., Norry, M., Willcox, C., 2012. Complex magma mixing, mingling, and withdrawal associated with an intraplinian ignimbrite eruption at a large silicic caldera volcano: Los Humeros of central Mexico. Geol. Soc. Am. Bull. 124, 1793–1809.
Carrasco-Núñez, G., Lopez-Martinez, M., Hernandez, J., Vargas, V., 2017a. Subsurface stratigraphy and its correlation with the surficial geology at Los Humeros geothermal field, eastern Trans-Mexican Volcanic Belt. Geothermics 67, 1–17.
Carrasco-Núñez, G., Hernández, J., De León, L., Dávila, P., Norini, G., Bernal, J.P., Jicha, B., Navarro, M., López, P., 2017b. Geologic map of Los Humeros volcanic complex and geothermal field, eastern Trans-Mexican Volcanic Belt. Terra Digitalis 1 (2), 1–11.
Carrasco-Núñez, G., Bernal, J.P., Davila, P., Jicha, B., Giordano, G., Hernandez, J., 2018. Reappraisal of Los Humeros volcanic complex by new U/Th zircon and 40Ar/39Ar dating: implications for greater geothermal potential. Geochem. Geophys. Geosyst. 19, 132–149.
Casique, J., García, S., Yáñez, C., Palacios, L.H., Garcia, H., 1982. Resultados de las exploraciones realizadas por CFE en el proyecto geotérmico Los Humeros-Derrumbadas, Estados de Puebla y Veracruz. An. Inst. Geofis. 27-28, 9–61.
Cedillo-Rodríguez, F., 1984. Estudio geologico de Los humeros-Las derrumbadas. Internal Report 17/84. Edos. De Pue. Y Ver. . Comision Federal de Electricidad, p. 55.
Cedillo-Rodríguez, F., 1997. Geologia del subsuelo del campo geotermico de Los Humeros, Pue. Internal Report HU/RE/03/97. Comision Federal De Electricidad, Gerencia De Proyectos Geotermoelectricos. Residencia Los Humeros, Puebla, p. 30.
Cedillo-Rodríguez, F., 1999. Modelo hidrogeológico de los yacimientos geotérmicos de Los Humeros, Puebla, México. Geotermia Revista Mexicana de Geoenergía 15, 159–170.
Cedillo-Rodríguez, F., 2000. Hydrogeologic model of the geothermal reservoir from Los Humeros, Puebla Mexico. Transactions – Geothermal Resources Council, pp. 433–436.
Chacko, T., Cole, D.R., Horita, J., 2001. Equilibrium oxygen, hydrogen and carbon isotope fractionation factors applicable to geologic systems. Rev. Mineral. Geochem. 43 (1), 1–81.
Chiodini, G., Marini, L., 1998. Hydrothermal gas equilibria: the H_2O-H_2-CO_2-CO-CH_4 system. Geoch. Cosmochi. Acta. 62 (15), 2673–2687.
Chiodini, O., Cioni, R., Guidi, m., Marmi, L., Raco, B., Taddeucci, G., 1992. Gas geobarometry in boiling hydrothermal systems: a possible tool to evaluate the hazard of hydrothermal explosions. Acta Vulcanol. 2, 99–107.
Chiodini, G., Cioni, R., Leonis, C., Marini, L., Raco, B., 1993. Fluid geochemistry in Nisyros island, dodecanese. Greece. J. Volcanol. Geotherm. Res. 56, 95–112.
Cioni, R., Corazza, E., Magro, G., Guidi, M., Marini, L., 1988. Reactive and inert gases in low temperature fumaroles (Aeolian Islands, Italy). Rend. Soc. Ita. Min. Petr., vol43 1003–1011.
Clark, I.D., Fritz, P., 1997. Environmental Isotopes in Hydrogelogy. CRC Press/Lewis Publishers, Boca Raton, Fl.
Craig, H., 1953. The geochemistry of the stable carbon isotopes. Geochim. Cosmochim. Acta 3, 53–92.
Craig, H., 1961. Isotopic variations in meteoric waters. Science 133 (3465), 1702–1703.
Craig, H., 1963. The isotopic geochemistry of water and carbon in geothermal areas. Nuclear Geology on Geothermal Areas, Spoleto, pp. 17–53, 1963.

D'Alessandro, W., Bellomo, S., Brusca, L., Fiebig, J., Longo, M., Martelli, M., Pecoraino, G., Salerno, F., 2009. Hydrothermal methane fluxes from the soil at Pantelleria island (Italy). J. Volcanol. Geoth. Res. 187, 147–157.
D'Amore, F., Panichi, C., 1987. Geochemistry in geothermal exploration. Appl. Geotherm. 9 (1987), 69–89.
Dávila-Harris, P., Carrasco-Núñez, G., 2014. An unusual syn–eruptive bimodal eruption: the Holocene Cuicuiltic Member at Los Humeros caldera, Mexico. J. Volcanol. Geotherm. Res. 271, 24–42.
De la Cruz, V., 1983. Estudio geológico a detalle de la zona geotérmica LosHumeros, Pue., Internal report 10/83. CFE, p. 51.
Des Marais, D.J., Stallard, M.L., Nehring, N.L., Truesdell, A.H., 1988. Carbon isotope geochemistry of hydrocarbons in the Cerro Prieto geothermal field, Baja California norte, Mexico. . Chem. Geol. 71, 159–167.
Doveri, M., Mussi, M., 2014. Water isotopes as environmental tracers for conceptual understanding of groundwater flow: an application for fractured aquifer systems in the "Scansano-Magliano in toscana" area (Southern Tuscany, Italy). Waters 6, 2255–2277.
Ferrara, G.C., Ferrara, G., Gonfiantini, R., 1963. Carbon isotopic composition of carbon dioxide and methane from steam jets of Tuscany. In: Tongiorgi, E. (Ed.), Nuclear Geology of Geothermal Areas, pp. 277–284. Pisa.
Ferrari, L., Orozco-Esquivel, T., Manea, V., Manea, M., 2012. The dynamic history of the Trans–Mexican Volcanic Belt and the Mexico subduction zone. Tectonophysics 522–523, 122–149.
Ferriz, H., Mahood, G., 1984. Eruption rates and compositional trends at Los Humeros volcanic center. Puebla, México. J. Geophys. Res. 89 (B10), 8511–8524.
Giggenbach, W.F., 1971. Isotopic composition of waters of the Broadlands geothermal field (New Zealand). NZ.J Sci. 14 (959-), 970.
Giggenbach, W.F., 1975. A simple method for the collection and analysis of volcanic gas samples. Bull. Volcanol. 39, 132–145.
Giggenbach, W.F., 1978. The isotopic composition of waters from the El Tatio geothermal field, Northern Chile. Geochim. Cosmochim. Acta 42 (979-), 988.
Giggenbach, W.F., 1980. Geothermal gas equilibria. Geoch. Cosmochim. Acta 44, 2021–2032.
Giggenbach, W.F., 1987. Redox processes governing the chemistry of fumarolic gas discharges from White Island, New Zealand. Appl. Geochem. 2 (2), 143–161.
Giggenbach, W.F., 1988. Geothermal solute equilibria. Derivation of NaKMgCa geoindicators. Geochim. Cosmochim. Acta 52, 27492765.
Giggenbach, W.F., 1992a. Isotopic shifts in waters from geothermal and volcanic systems along convergent plate boundaries and their origin. Earth Planet. Sci. Lett. 113, 495–510.
Giggenbach, W.F., 1992b. Magma degassing and mineral deposition in hydrothermal systems along convergent plate boundaries. Econ. Geol. 87, 1927–1944.
Giggenbach, W.F., 1993. Reply to comment by P. Blattner: "Andesitic water": a phantom of the isotopic evolution of water-silicate systems. Earth Planet. Sci. Lett. 120, 519–522.
Giggenbach, W.F., 1997. The origin and evolution of fluids in magmatic-hydrothermal systems. In: Barnes, H.L. (Ed.), Geochemistry of Hydrothermal Ore Deposits, 3d edition. Wiley, pp. 737–796.
Giggenbach, W.F., Poreda, R.J., 1993. Helium isotopic and chemical composition of gases from volcanic–hydrothermal systems in the Philippines. Geothermics 22, 369–380.
Giggenbach, W.F., Stewart, M.K., 1982. Processes controlling the isotopic composition of steam and water discharges from steam vents and steam-heated pools in geothermal areas. Geothermics 11 (2), 71–80.
Giggenbach, W.F., Sano, Y., Wakita, H., 1993. Isotopic composition of helium, and CO_2 and CH_4 contents in gases produced along the New Zealand part of a convergent plate boundary. Geochim. Cosmochim. Acta 57, 3427–3455.
Giroud, N., 2008. A Chemical Study of Arsenic, Boron and Gases in High-temperature Geothermal Fluids in Iceland. PhD Thesis. University of Iceland, Reykjavik, Iceland, p. 110. ISBN 978-9979-70-479-9.
González-Partida, E., Barragán, R., Nieva, D., 1993. Análisis geoquímico-isotópico de las especies carbónicas del fluido geotérmico de Los Humeros, Puebla, México. Geofis. Int. 32, 299–309.
Gudmundsson, B.Th., Arnórsson, S., 2002. Geochemical monitoring of the Krafla and Namafjall geothermal areas, N-Iceland. Geothermics 31, 195–243.
Gunter, B.D., Musgrave, B.C., 1971. New evidence on the origin of methane in hydrothermal gases. Geochim. Cosmochim. Acta 35, 113–118.
Gutiérrez-Negrín, L.C.A., 2019. Current status of geothermal-electric production in Mexico. IOP Conf. Ser.: Earth Environ. Sci. 249, 012017.
Gutiérrez-Negrín, L.C.A., Izquierdo-Montalvo, G., 2010. Review and update of the main features of the Los Humeros geothermal field, Mexico. In: Proceedings World Geothermal Congress 2010. Bali, Indonesia, p. 7, 25-29 April 2010.
Hedenquist, J.W., 1986. Geothermal systems in the Taupo volcanic zone; Their characteristics and relation to volcanism and mineralisation. In: Smith, I.E.M. (Ed.), Late Cenozoic Volcanism in New Zealand. Bulletin – Royal Society of New Zealand, pp. 134–168, 23.
Hedenquist, J.W., Lowenstern, J.B., 1994. The role of magmas in the formation of hydrothermal ore deposits. Nature 370, 519–526.
Henley, R.W., Ellis, A.J., 1983. Geothermal systems ancient and modern: a geochemical review. Earth. Rev. 19 (1), 1–50.
Henley, R.W., Truesdell, A.H., Barton Jr, P.B., 1984. In: Robertson, J. (Ed.), Fluid Mineral Equilibria in Hydrothermal Systems. Society of Economic Geologist.
Horita, J., Wesolowski, D.J., 1994. Liquid-vapor fractionation of oxygen and hydrogen isotopes of water from the freezing to the critical temperature. Geochim. Cosmochim. Acta 58, 3425–3437. https://doi.org/10.1016/0016-7037(94)90096-5.
Hulston, J.R., McCabe, W.J., 1962a. Mass spectrometer measurements in the thermal areas of New Zealand, part 1. Carbon dioxide and residual gas analyses. Geochim. Cosmochim. Acta 26, 383–397.
Hulston, J.R., McCabe, W.J., 1962b. Mass spectrometer measurements in the thermal areas of New Zealand, part 2. Carbon isotope ratios. Geochim. Cosmochim. Acta 26, 399–410.
Issar, A., Quijano, J.L., Gat, J.R., Castro, M., 1984. The isotope hydrology of the groundwaters of central Mexico. J. Hydrol. (Amst) 71, 201–224.
Karingithi, C.W., Arnórsson, S., Gronvold, K., 2010. Processes controlling aquifer fluid compositions in the Olkaria geothermal system. Kenya. Journal of Volcanology and Geothermal Research 196, 57–76.
Langmuir, C.H., Vocke Jr., R.D., Hanson, G.N., Hart, S.R., 1978. A general mixing equation with applications to Icelandic basalts. Earth Planet. Sci. Lett. 37, 380–392.
López-Hernández, A., 1995. Estudio regional volcanico y estructural del Campo Geotermico De Los Humeros, Pue., Mexico. Geotermia Rev. Mex. de Geoenergia 11 (1), 17–36.
Lorenzo-Pulido, C.D., 2008. Borehole geophysics and geology of well H-43, Los Humeros geothermal field, Puebla, México. Geother. Tra. Program.Rep. 9, 23. Orkustofnun, Grensásvegur, Reykjavík, Iceland.
Lyon, G.L., Hulston, J.R., 1984. Carbon and hydrogen isotopic compositions of New Zealand geothermal gases. Geochim. Cosmochim. Acta 48, 1161–1171.
Magro, G., Ruggieri, G., Gianelli, G., Bellani, S., Scandiffio, G., 2003. Helium isotopes in paleofluids and present-day fluids of the §Larderello geothermal field: constraints on the heat source. J. Geophy. Res. 108 (B1) doi:10.1029/2001JB001590, 2003.
Mnjokava, T., Kimani, A., Pasqua, C., Lelli, M., Marini, L., 2018. Geochemistry of kilambo-kajala and ilwalilo Hot Springs, kiejo-mbaka geothermal Prospect, Tanzania. In: Proceedings, 7th African Rift Geothermal Conference. Kigali, Rwanda, 31st October – 2nd November 2018.
Naumov, B., Ryzhenko, B.N., Khodakovsky, I.L., 1974. Handbook of Thermodynamic Data. U.S.G.S.WRD-74001, NTIS PB-226722/AS.
Norini, G., Groppelli, G., Sulpizio, R., Carrasco-Núñez, G., Dávila-Harris, P., Pellicioli, C., Zucca, F., De Franco, R., 2015. Structural analysis and thermal remote sensing of the Los Humeros Volcanic Complex: implications for volcano structure and geothermal exploration. J. Volcanol. Geotherm. Res. 301, 221–237.
Ohmoto, H., 1986. Stable isotope geochemistry of ore deposits. In: Valley, J.W., Taylor, H.P., O'Neil, J.R. (Eds.), Stable Isotopes in High Temperature Geological Processes, Reviews in Mineralogy, pp. 491–559, 16.
Peiffer, L., Carrasco Núñez, G., Mazot, A., Villanueva-Estrada, R.E., Inguaggiato, C., Romero, R.B., Rocha Miller, R., Hernández Rojas, J., 2018. Soil degassing at the Los Humeros geothermal field (Mexico). J. Volc. Geoth. Res. 356, 163–174.
Pinti, D.L., Marty, B., 1998. The origin of helium in deep sedimentary aquifers and the problem of dating very old groundwaters. Geol. Soc. Lond. Spec. Publ. 144, 53–68.
Pinti, D.L., Castro, M.C., Shouakar-Stash, O., Tremblay, A., Garduño, V.H., Hall, C.M., Hélie, J.-F., Ghaleb, B., 2013. Evolution of the geothermal fluids at Los Azufres, Mexico, as traced by noble gas isotopes, $\delta^{18}O$, δD, $\delta^{13}C$ and $^{87}Sr/^{86}Sr$. J. Volcanol. Geotherm. Res. 249, 1–11.
Pinti, D.L., Castro, M.C., Lopez-Hernández, A., Han, G., Shouakar-Stash, O., Hall, Ch.M., Ramírez-Montes, M., 2017. Fluid circulation and reservoir conditions of the Los Humeros Geotermal Field (LHCF), México, as revealed by a noble gas survey. J. Volcanol. Geotherm. Res. 333-334, 104–115.
Pope, E.C., Bird, D.K., Arnórsson, S., Giroud, N., 2016. Hydrogeology of the Krafla geothermal system, northeast Iceland. Geofluids 16, 175–197. https://doi.org/10.1111/gfl.12142.
Poreda, R., Craig, H., 1989. Helium isotopes ratios in circum-Pacific volcanic arcs. Nature 338, 473–478.
Poreda, R.J., Craig, H., Arnórsson, S., Welhan, J.A., 1992. Helium isotopes in Icelandic geothermal systems 1. 3He, gas chemistry and 13C relations. Geochim. Cosmochim. Acta 56, 4221–4228.
Portugal, E., Verma, M.P., Barragán, R.M., Mañón, A., 1994. Geoquímica isotópica de ^{13}C, D y ^{18}O de fluidos del sistema geotérmico Los Humeros, Puebla (México). Geofisica Int. 33 (4), 607–618.
Prol-Ledesma, R.M., 1998. Pre- and post-exploration variations in hydrothermal activity in Los Humeros geothermal field, Mexico. J. Volcanol. Geotherm. Res. 83, 313–333.
Richard, L., Pinti, D.L., Hélie, J.-F., Lopez Hernandez, A., Shibata, T., Castro, M.C., Sano, Y., Shouakar-Stash, O., Sandoval-Medina, F., 2019. Variability of deep sources in Mexican geothermal fluids. J. Volcanol. Geoth. Res 370, 1–12.
Romero, F., 1991. Los Humeros geothermal field, Puebla. In: De Salas, G.P. (Ed.), Economical Geology, Vol. P-3. Geological Society America, Mexico, pp. 77–94. Boulder, CO, The Geology of North America.
Ryzhenko, B.N., Malinin, S.D., 1971. The fugacity rule for the systems CO_2-H_20, CO_2-CH_4, CO_2-N_2, and CO_2-H_2. Geochem. Int., p. 562–574.
Ryzhenko, B.N., Volkov, V.P., 1971. Fugacity coefficients of some gases over a broad range of temperatures and pressures. Geochem. Int., p. 468–481.
Sano, Y., Marty, B., 1995. Origin of carbon in fumarolic gas from island arcs. Chem. Geol. 119, 265–274.
Sano, Y., Wakita, H., 1985. Geographical distribution of 3He/4He ratios in Japan: implications for arc tectonics and incipient magmatism. J. Geophys. Res. 90, 8729–8741.
Schoell, M., 1980. The hydrogen and carbon isotopic composition of methane from natural gases of various origins. Geochim. Cosmochim. Acta 44 (5), 649–661.
Schoell, M., 1988. Multiple origins of methane in the earth. In: Origins of Methane in the Earth (Schoell Ed.). Chem. Geol, Volume 71, pp. 1–10.
Taylor Jr, H.P., 1971. Oxygen isotope evidence for large-scale interaction between meteoric ground waters and Tertiary granodiorite intrusions, western cascade range, oregon. J. Geophys. Res. 76 (32), 7855–7874.

Taylor, H.P.J.R., 1977. Water/rock interactions and the origin of H_2O in granitic batholith. J. Geol. Soc. Lond. 133, 509–558.

Taylor, H.P.J.R., 1979. Oxygen and hydrogen isotope relationships in hydrothermal mineral deposits. In: Barnes, H.L. (Ed.), Geochemistry of Hydrothermal Ore Deposits, 2nd edition. John Wiley, New York, pp. 236–277.

Tello, H.E., 1990. Características geoquímicas e isotópicas de los fluidos producidos por los pozos de Los Humeros, Puebla, México. In: Geothermal Investigations with Isotope and Geochemical Techniques in Latin America, Proceedings of a Final Research Co-Ordination Meeting. San José, Costa Rica, pp. 307–344, 12-16 November 1990.

Tello, H.E., Verma, M.P., Tovar, R.A., 2000. Origin of acidity in the Los Humeros, Mexico, geothermal reservoir. In: Proceedings World Geothermal Congress. Japan. May 28-June 10.

Tello, H.E., Tovar, R.A., Verma, M.P., 2005. Chemical and isotopic study to define the origin of acidity in the los humeros geothermal reservoir. Use of Isotope Techniques to Trace the Origin of Acidic Fluids in Geothermal Systems. IAEA-TECDOC-1448, Vienna (April 2005), ISBN 92–0–102805–102809.

Torres-Alvarado, I.S., Satir, M., Pérez-Zarate, D., Birkle, P., 2012. Stable isotope composition of hydrothermally altered rocks and hydrothermal minerals at the Los Azufres geothermal field, Mexico. Turk. J. Earth Sci. 21, 127–143.

Truesdell, A.H., 1991a. The origin of high-temperature zones in vapor-dominated geothermal systems. In: Proc. Sixteenth Workshop on Geotherm. Res. Eng., Stanford Univ. Stanford, CA, pp. 15–20.

Truesdell, A.H., 1991b. Origins of acid fuids in geothermal reservoirs. Geotherm. Res. Counc. Trans. 15, 289–296.

Truesdell, A.H., Hulston, J.R., 1980. Isotopic evidence on environments of geothermal systems. In: Fonteg, Fritz (Eds.), Handbook of Environmental Isotope Geochemistry, Volume 1. Elsevier, Amsterdam.

Truesdell, A.H., Nathenson, M., Rye, R.O., 1977. The effects of subsurface boiling and dilution on the isotopic composition of Yellowstone thermal waters. J. Geophys. Res. 82 (3694-), 3704.

Welhan, J.A., 1988. Origins of methane in hydrothermal systems. Chem. Geol. 71 (1-3), 183–198.

Yáñez, C., Garcia, S., 1982. Exploracion de la region geotermica Los Humeros-Las Derrumbadas. Internal Report 29/82. Estados de Puebla y Veracruz. Comision Federal de Electricidad, p. 98.